Frustration shapes multi-channel Kondo physics: A star graph perspective

Siddhartha Patra,[1, *] Abhirup Mukherjee,[1, †] Anirban Mukherjee,[1, ‡]
N. S. Vidhyadhiraja,[2, §] A. Taraphder,[3, ¶] and Siddhartha Lal[1, **]

[1]*Department of Physical Sciences, Indian Institute of Science Education and Research-Kolkata, W.B. 741246, India*
[2]*Theoretical Sciences Unit, Jawaharlal Nehru Center for Advanced Scientific Research, Jakkur, Bengaluru 560064, India*
[3]*Department of Physics, Indian Institute of Technology Kharagpur, Kharagpur 721302, India*

(Dated: April 26, 2022)

Our study of the multi-channel Kondo (MCK) model using the recently developed unitary renormalization group (URG) technique shows the importance of ground state degeneracy in explaining various important properties like the breakdown of screening and the presence of local non-Fermi liquids. The impurity susceptibility of the zero-bandwidth intermediate coupling fixed point Hamiltonian shows power-law divergence at low temperature, signaling its critical nature. Despite the absence of inter-channel coupling in the MCK Hamiltonian, the study of mutual information between two channels shows non-zero correlation among them. The presence of non-local twist and translation operators shows the topological nature of the degenerate ground state manifold. Upon disentangling the impurity spin, we find the presence of local Mott-liquid made out of inter-channel quantum scatterings. We derive the low energy effective Hamiltonian (LEH) upon the addition of excitation to the zero-bandwidth RG fixed point Hamiltonian for the two and three-channel cases, both of which show the absence of local Fermi liquid phase due to exact cancellation coming from different degenerate ground states, and the presence of non-Fermi liquids with inter-channel quantum fluctuations. Computation of various thermodynamic quantities like specific heat and susceptibility in the ground state of that non-Fermi liquid shows logarithmic scaling in low temperature, which agrees with the known result in the literature. The presence of local marginal Fermi liquid shows the orthogonality catastrophe in the two-channel Kondo model. Discontinuity in various entanglement measures as we add the excitations on top of the zero-bandwidth model by tuning the real space nearest-neighbor hopping strength reinforces the presence of orthogonality catastrophe. Strong and weak coupling duality also sheds light on the presence of an intermediate coupling fixed point in the MCK problem. The study of channel anisotropy under URG reveals series of quantum phase transitions due to the change in ground state degeneracy. Our work thus shows a template of studying the zero-bandwidth model followed by the systematic addition of excitations, which can be used to study other impurity problems.

I. INTRODUCTION

Local antiferromagnetic exchange interaction between a spin-$\frac{1}{2}$ impurity and a metal gives rise to the well-understood phenomenon of Kondo effect [1]. Here, the impurity local moment is screened by the conduction electrons at temperatures below a certain scale called the Kondo temperature [2–9], leading to a spin singlet ground state and local Fermi liquid excitations above that ground state [10, 11]. The screening manifests as an initial increase at temperatures below the Kondo temperature, followed by a saturation of the resistivity of the metal [12, 13], and in the saturation of the impurity contribution to the magnetic susceptibility at low temperatures [5–7]. Generalisations of this model are obtained by taking impurities of higher spin [1, 8, 14], adding interactions between them [15–21], by promoting to a Kondo lattice of impurities [22–26] or by considering a correlated metal [27]. One can also construct multi-channel Kondo (MCK) models by allowing K conduction electron channels ($K > 1$) to interact with a spin-$\frac{1}{2}$ impurity (S_d) [14, 28, 29] via a common exchange coupling $\mathcal{J}$. Using conformal field theory [8, 30–34], bosonization [35–39], numerical renormalization group [32, 40, 41], Bethe ansatz [42–46] and other methods [47–50], it has been shown that for the over-screened systems ($K > 2S_d$), the low energy physics is of the non-Fermi liquid type, displaying anomalous behaviour in thermodynamic properties near $T = 0$ and a fractional zero temperature entropy in the thermodynamic limit (ensuring that temperature is taken to zero before the system size is taken to infinity [38, 51]). This anomalous divergent behaviour is actually a signature of the fact that the MCK system with a single channel-symmetric exchange coupling is quantum critical: it is susceptible to perturbations that introduce channel isotropy in the exchange couplings [14, 32, 37, 45, 52]. This makes the experimental realisation of such states quite challenging. Nevertheless, several features of the two-channel Kondo model have been reproduced using structural two-level systems [28, 53] interacting with a conduction bath [54–58]. More recently, it has become possible to tune a two-channel quantum dot system across the quantum phase transition [59, 60], revealing the fractionalisation of the

* sp14ip022@iiserkol.ac.in
† am18ip014@iiserkol.ac.in
‡ mukherjee.anirban.anirban@gmail.com
§ raja@jncasr.ac.in
¶ arghya@phy.iitkgp.ernet.in
** slal@iiserkol.ac.in

low-energy degrees of freedom [49, 61, 62].

The importance of ground state degeneracy and quantum-mechanical frustration in the MCK problem has not received sufficient attention, even though they play crucial roles in determining the non-Fermi liquid physics and the quantum criticality of the system. This is, at least partially, due to the lack of an intermediate-coupling effective Hamiltonian that describes the low-energy physics of the MCK (i.e., reveals the nature of the excitations). The term frustration in this context refers to the inability of the impurity spin to bind with the conduction channels and get completely screened by forming a maximally-entangled singlet. The absence of such frustration in the single-channel spin-1/2 Kondo model (and more generally, the exact screening variant of the MCK) means that imperfect screening ($K \neq 2S_d$) should lead to dramatic differences in the multi-channel models. Indeed, we demonstrate that there exists an orthogonality catastrophe in the imperfectly screened MCK models leading to the non-Fermi liquid behaviour of its low-energy excitations, and that it is directly related to the existence of a degenerate ground state manifold. The effects of these non-Fermi liquid low energy excitations are expected to show up in measures of many-particle entanglement; the lack of an intermediate coupling Hamiltonian has, however, prevented the study of the renormalisation group (RG) evolution of such measures [63, 64]. Our approach enables a comparison of, for instance, the inter-channel mutual information along the RG flow and as functions of the excitation energies, providing insight into the nature of the fixed point theory.

To obtain the RG flow of the MCK model, we have employed the recently developed unitary renormalization group (URG) technique [65, 66]. The method has been applied on several fermionic and spin problems like the single-channel Kondo model [67], the kagome antiferromagnet [68], the 1D [69] and 2D Hubbard models [70, 71], the reduced-BCS model [72] as well as other generalised models of interacting electrons with and without translation invariance [66]. The URG proceeds by decoupling number fluctuations in the high energy electronic states. Iteratively applying this URG method on the channel-isotropic MCK model leads to a low energy fixed point Hamiltonian at intermediate Kondo coupling. In further analysing the effective Hamiltonian, we focus initially on the zero bandwidth limit of this Hamiltonian (which corresponds to a frustrated quantum spin model on a star graph). We show thereby that several important properties of the MCK problem, such as the ground state degeneracy and breakdown of screening, can be understood from the zero bandwidth problem. We then proceed to studying the low energy effective Hamiltonian for the non-Fermi liquid excitations lying above the degenerate ground state manifold. This enables the computation of a plethora of quantities, such as various thermodynamic measures (e.g., specific heat and susceptibility), many-particle entanglement and the self-energy of the propagating degrees of freedom. We also explore various signatures of criticality, and various duality transformations of the MCK Hamiltonian. Finally, we investigate the evolution of ground state degeneracy under RG of the channel anisotropic MCK model.

Summary of Main Results

We start in section II by describing the URG flows for the MCK, the intermediate coupling URG fixed point Hamiltonian and the features of the zero bandwidth (star graph) limit of the effective Hamiltonian. In section III, we explore some properties of the zero bandwidth model: namely, the degree of compensation, impurity magnetisation and impurity susceptibility. The degree of compensation is simply the average correlation between the impurity spin and the conduction channel local spins; it is found to be maximum at exact screening, and decreases for both over- and under-screening. The magnetisation and susceptibility of the star graph model show critical behaviour in the form a discontinuity and a T^{-1} divergence respectively. We also explore the topological properties of the degenerate ground state manifold of the star graph model using non-local twist and translation operators. On decoupling the impurity spin from the conduction spin degrees of freedom within the star graph, we obtain an all-to-all Hamiltonian that represents a local Mott liquid phase. In section IV, we obtain the low energy effective Hamiltonian for the low-lying excitations by including a dispersion into the conduction bath. Notable features of this effective Hamiltonian include (i) the complete absence of local Fermi liquid terms, and (ii) the emergence of local non-Fermi liquid terms. Both are shown to result from the ground state degeneracy of the underlying star graph model. The excitations of the two-channel Kondo problem are found to pertain to a local marginal Fermi liquid, signalling an orthogonality catastrophe.

In section V, we study various entanglement signatures (like the von-Neumann entanglement entropy, mutual information, multipartite information, Bures distance) of the low energy fixed-point ground state of the MCK problem, with and without excitations. They reveal clear distinctions between the single- and MCK problems in the form of discontinuities. In VI, we discuss two duality transformations that exist for the MCK model - a strong-weak duality and an over-screened-under-screened duality. It is found that the transformations are constrained by the fixed point structure, and they impose relations between the under-screened and over-screened models. In VII, we show the robustness of the ground state degeneracy of the star graph model against the impurity-channel coupling anisotropy, and correlate it with a URG treatment of the channel anisotropic MCK. The isotropic fixed point is found to be unstable to asymmetry, leading to impurity phase transitions that lead to dramatic changes in the ground state degeneracy. For the sake of brevity, some supporting evidence and details of certain lengthy calculations are presented in Supplementary Materials [73].

II. FIXED POINT THEORY OF OVER-SCREENED MCK MODEL

A. RG flows towards intermediate coupling

We start with the K- conduction channel Kondo model Hamiltonian with isotropic couplings [14]:

$$H = \sum_{l}\Bigg[\sum_{\substack{k\\ \alpha=\uparrow,\downarrow}} \epsilon_{k,l}\hat{n}_{k\alpha,l} + \frac{\mathcal{J}}{2}\sum_{\substack{kk'\\ \alpha,\beta=\uparrow,\downarrow}} \vec{S}_d\cdot\vec{\sigma}_{\alpha\alpha'}c^\dagger_{k\alpha,l}c_{k'\alpha',l}\Bigg] , \tag{1}$$

where $\mathcal{J}$ is the Kondo spin-exchange coupling, $c_{k\alpha,l}$ is the fermionic field operator at momentum k, spin α and channel l, $\epsilon_{k,l}$ represents the dispersion of the l^{th} conduction channel, $\vec{\sigma}$ is the vector of Pauli matrices and $\vec{S}_d = \frac{1}{2}\vec{\sigma}_d$ is the impurity spin operator. Here, l sums over the K channels of the conduction bath, k, k' sum over all the momentum states of the bath and α, β sum over the two spin indices of a single electron.

We now perform a renormalisation group analysis of the MCK Hamiltonian using the recently developed URG method [65, 66, 68–72]. The RG proceeds by applying unitary transformations in order to block-diagonalize the Hamiltonian by removing number fluctuations of the high energy degrees of freedom. Given the most energetic electronic state at the j^{th} RG step is $|j\rangle$ and defined by the energy $D_{(j)}$, the Hamiltonian will in general not conserve the number of particles in this state: $\left[H_{(j)}, \hat{n}_j\right] \neq 0$. The unitary transformation $U_{(j)}$ will remove this number fluctuation at the next RG step [65, 66]:

$$H_{(j-1)} = U_{(j)}H_{(j)}U^\dagger_{(j)} \ , \ \ \left[H_{(j-1)}, \hat{n}_j\right] = 0 \ . \tag{2}$$

The unitary transformations are given in terms of a fermionic generator $\eta_{(j)}$ [65, 66]:

$$U_{(j)} = \frac{1}{\sqrt{2}}\left(1 + \eta_{(j)} - \eta^\dagger_{(j)}\right) \ , \qquad \left\{\eta_{(j)}, \eta^\dagger_{(j)}\right\}_\pm = 1 \ , \tag{3}$$

where $\{A, B\}_\pm = AB \pm BA$. The generator itself is given by the expression [65, 66]

$$\eta^\dagger_{(j)} = \frac{1}{\hat{\omega}_{(j)} - \text{Tr}\left(H_{(j)}\hat{n}_j\right)} c^\dagger_j \text{Tr}\left(H_{(j)}c_j\right) \ . \tag{4}$$

The operator $\hat{\omega}_{(j)}$ encodes the quantum fluctuation scales arising from the interplay of the kinetic energy terms and the interaction terms in the Hamiltonian:

$$\hat{\omega}_{(j)} = H_{(j-1)} - H^i_{(j)} \ . \tag{5}$$

$H^i_{(j)}$ is that part of $H_{(j)}$ that commutes with $\hat{n}_j$ but does not commute with at least one $\hat{n}_l$ for $l < j$. The RG flow continues up to energy D^*, where a fixed point is reached from the vanishing of the RG function.

The derivation of the RG equation for the over-screened regime ($2S < K$) of the spin-S-impurity K-channel Kondo problem is shown in detail in the Supplementary Materials (CITE). On decoupling circular isoenergetic shells at energies $D_{(j)}$, the change in the Kondo coupling at the j^{th} RG step, $\Delta\mathcal{J}_{(j)}$, is given by

$$\Delta\mathcal{J}_{(j)} = -\frac{\mathcal{J}^2_{(j)}\mathcal{N}_{(j)}}{\omega_{(j)} - \frac{D_{(j)}}{2} + \frac{\mathcal{J}_{(j)}}{4}}\left(1 - \frac{1}{2}\rho\mathcal{J}_{(j)}K\right) \ , \tag{6}$$

where $\mathcal{N}_{(j)}$ is the number of electronic states at the energy shell $D_{(j)}$. We work in the low quantum fluctuation regime $\omega_{(j)} < \frac{D_{(j)}}{2}$. There are three fixed points of the RG equation. One arises from the vanishing of the denominator, and was present in the single-channel Kondo RG equation as well [67]. As shown there, this fixed-point goes to $\mathcal{J}^* = \infty$ as the bare bandwidth of the conduction electrons is made large. The other trivial fixed point is the trivial one at $\mathcal{J}^* = 0$. The third fixed point is reached when the numerator vanishes: $\mathcal{J}^* = \frac{2}{K\rho}$ [14, 74–76]. Only the intermediate fixed point is found to be stable. This is consistent with results from Bethe ansatz calculations [42–46, 77], CFT calculations [8, 30, 31], bosonization treatments [35, 38] and NRG analysis [41, 78].

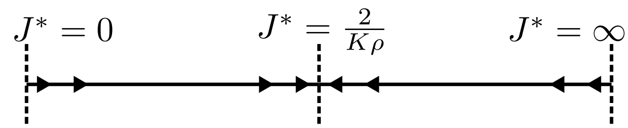

FIG. 1. The three fixed points of the over-screened RG equation. Only the intermediate one is stable.

The RG equation reduces to the perturbative form $\Delta\mathcal{J}_{(j)} \simeq \frac{\mathcal{J}^2_{(j)}\mathcal{N}_{(j)}}{D_{(j)}}\left(1 - \frac{1}{2}\rho\mathcal{J}_{(j)}K\right)$ [14, 75, 76, 79] when one replaces $\omega_{(j)}$ with the ground state energy $-\frac{D_{(j)}}{2}$ and assumes $\mathcal{J} \ll D_{(j)}$.

B. The star graph as the zero-bandwidth limit of the fixed point Hamiltonian

The fixed point Hamiltonian takes the form

$$H^* = \sum_{l}\left[\sum_{k}^{*}\epsilon_{k,l}\hat{n}_{k\alpha,l} + \mathcal{J}\sum_{kk'}^{*}\vec{S}_d\cdot\frac{1}{2}\vec{\sigma}_{\alpha\alpha'}c^\dagger_{k\alpha,l}c_{k'\alpha',l}\right] . \tag{7}$$

We have not explicitly written the decoupled degrees of freedom $D_{(j)} > D^*$ in the Hamiltonian. The $*$ over the summations indicate that only the momenta inside the window D^* enter the summation. There is an implied summation over the spin indices α, β.

We will first study the zero bandwidth limit of the fixed point Hamiltonian, obtained by compressing the sum over the momentum states to a single state at the Fermi surface. Upon setting the chemical potential equal to the Fermi energy, the kinetic energy part vanishes and the zero bandwidth model becomes a Heisenberg spin-exchange Hamiltonian.

$$H^* = \mathcal{J}\sum_l \sum_{kk'}^* \vec{S}_d \cdot \frac{1}{2}\vec{\sigma}_{\alpha\alpha'} c^\dagger_{k\alpha,l} c_{k'\alpha',l} = \mathcal{J}\vec{S}_d \cdot \vec{S} \ . \quad (8)$$

At the last step, we defined the total bath local spin operator $S = \sum_l \vec{S}_l = \frac{1}{2}\sigma_l = \frac{1}{2}\sum^*_{kk'}\sum_{\alpha\beta}\vec{\sigma}_{\alpha\alpha'} c^\dagger_{k\alpha,l} c_{k'\alpha',l}$. The star graph commutes with several operators, includ-

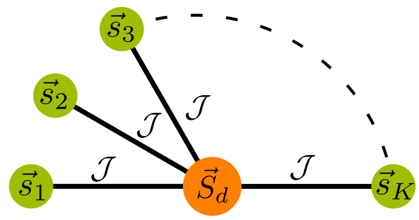

FIG. 2. Zero bandwidth limit of the fixed point Hamiltonian. The central yellow node is the impurity; it is interacting with the K green outer nodes that represent the local spins of the channels.

ing the total spin operator $J^z = S^z_d + S^z$ along z, the total bath local spin operator S^2 and the string operators

$$\pi^{x,y,z} = \sigma_d^{x,y,z} \otimes_{l=1}^K \sigma_l^{x,y,z} \ . \quad (9)$$

If we define the global spin operator $\vec{J} = \vec{S} + \vec{S}_d$, the star graph Hamiltonian can be written as $\frac{1}{2}\mathcal{J}\left[J^2 - S_d^2 - S^2\right]$.

- The ground state is achieved for the maximal value of S, $S = \frac{K}{2}$, and the corresponding minimal value of J, $J = |\frac{K}{2} - S_d|$. The ground state energy is therefore

$$\begin{aligned} E_g &= \frac{1}{2}\mathcal{J}\left[J(J+1) - S_d(S_d+1) - S(S+1)\right] \\ &= \begin{cases} -\mathcal{J}S_d\left(\frac{K}{2}+1\right) & \text{when } K \geq 2S_d, \text{ and} \\ -\mathcal{J}\frac{K}{2}\left(S_d+1\right) & \text{otherwise .} \end{cases} \end{aligned} \quad (10)$$

- The value of J corresponds to a multiplicity of $2J + 1 = |K - 2S_d| + 1$ in J^z, and since the Hamiltonian does not depend on J^z, these orthogonal states $|J^z\rangle$ constitute a degeneracy of $g_K^{S_d} = |K - 2S_d| + 1$.

The π^z acts on the eigenstates $|J^z\rangle$ and reveals the odd-even parity of the eigenvalue J^z, and is hence a parity operator. Interestingly, the string operator π^z is a Wilson loop operator [80] that wraps around all the nodes of the star graph:

$$\pi^z = \exp\left[i\frac{\pi}{2}\left(\sigma_d^z + \sum_{l=1}^K \sigma_l^z - K\right)\right] = e^{i\pi\left(J^z - \frac{1}{2}K\right)} \ . \quad (11)$$

π^x and π^y are 't Hooft operators [80] and mix states of opposite parity. For example, it can be shown that $\pi^x|J^z\rangle = -|J^z\rangle$.

There are several reasons for working with the star graph in particular and zero mode Hamiltonians in general. In the single-channel Kondo model, the star graph is just the two spin Heisenberg, and it reveals the stabilization of the Kondo model ground state, as well as certain thermodynamic properties (e.g., the impurity contribution to the susceptibility) [67, 81–84]. Similarly in the MCK model, the star graph is able to mimic the nature of the RG flows. At weak coupling $\mathcal{J} \to 0^+$, the central spin is weakly coupled to the outer spins and prone to screening because of the $S^\pm$ terms in the star graph; at strong coupling $\mathcal{J} \to \infty^-$, the outer spin-half objects tightly bind with the central spin-half object to form a single spin object that interacts with the remaining states through an exchange coupling which is RG relevant. This renders both the terminal fixed points unstable. The true stable fixed point must then lie somewhere in between, and we recover the schematic phase diagram of fig. 1.

Moreover, the RG flows of the MCK model have been show to preserve the degeneracy of the ground state [41, 85, 86], and the star graph captures this degeneracy in its entirety. This is important, because it will be shown in a later section that the lowest excitations of the intermediate fixed point is described a non-Fermi liquid phase, and it can be argued that this non-Fermi liquid physics arises solely from the ground state degeneracy of the underlying zero mode Hamiltonian. As mentioned previously, the ground state degeneracy of the more general star graph with a spin-S_d impurity and K channels is given by $g_K^{S_d} = |K - 2S_d| + 1$. The cases of $K = 2S_d$, $K < 2S_d$ and $K > 2S_d$ correspond to exactly screened, under-screened and over-screened regimes respectively. The latter two cases correspond to a multiply-degenerate manifold $g_K^S > 1$, and simultaneously have non-Fermi liquid phases [8, 14, 30, 33, 35, 49, 74, 77, 87–95], while the first regime has a unique ground state $g_K^S = 1$ and is described by a local Fermi liquid (LFL) phase [5–7, 10, 14], thereby substantiating the claim that a degeneracy greater than unity is closely tied to non-Fermi liquid physics.

In the following sections, we will show how the inherent quantum-mechanical frustration of singlet order that is present in the Hamiltonian leads to the non-trivial physics of the fixed points in terms of non-Fermi liquid phase, diverging thermodynamic quantities, quantum criticality as well as emergent gauge theories.

III. IMPORTANT PROPERTIES OF THE STAR GRAPH

A. Degree of compensation: a measure of the frustration

One can quantify the amount of screening of the local moment at the impurity site by defining a degree of compensation κ. Such a quantity also measures the inherent singlet frustration in the problem: the higher the degree of compensation, the better the spin can be screened into a singlet and lower is the frustration. It is given by the antiferromagnetic correlation existing between the impurity spin and conduction electron channels: $\Gamma \equiv -\left\langle \vec{S_d}\cdot\vec{S}\right\rangle$. The expectation value is calculated in the ground state. Since the inner product is simply the ground state energy of a spin-S impurity $K-$channel MCK model in units of the exchange coupling J, we have $\Gamma = \frac{1}{2}\left[l_{\text{imp}}^2 + l_c^2 - g_K^S\left(g_K^S - 1\right)\right]$, where $l_{\text{imp}}^2 = S_d(S_d+1)$ is the length-squared of the impurity spin. Similarly, $l_c^2 = \frac{K}{2}\left(\frac{K}{2}+1\right)$ is the length-squared of the total conduction bath spin. $g_K^S = |K - S_d| + 1$ is the ground state degeneracy. We will explore the three regimes of screening by defining $K = K_0 + \delta, S = \frac{K_0}{2} - \delta$. $\delta = 0$ represents the exactly-screened case of $K = 2S = K_0$. Non-zero δ represents either over- or under-screening. In terms of K_0 and δ, the degree of compensation becomes

$$\Gamma = \frac{1}{4}\left[\left(K_0+1\right)^2 - \left(|\delta|+1\right)^2\right] . \tag{12}$$

For a given K_0, the degree of compensation is maximised for exact screening $\delta = 0$, and is reduced for $\delta \neq 0$. This shows the inability of the system to form a unique singlet ground state and reveals the quantum-mechanical frustration inherent in the zero mode Hamiltonian and therefore in the entire problem. The degree of compensation is symmetric under the Hamiltonian transformation $\delta \to -\delta$, and this represents a duality transformation between over-screened and under-screened MCK models. This topic will be discussed in more detail later.

B. Impurity magnetization and susceptibility

In order to obtain the magnetic susceptibility, We insert a magnetic field that acts only on the impurity and then diagonalize the Hamiltonian.

$$H(h) = \mathcal{J}^*\vec{S_d}\cdot\vec{S} + hS_d^z \tag{13}$$

The Hamiltonian commutes with S, so it is already block-diagonal in terms of the eigenvalues M of S. M takes values in the range $[M_{\text{min}}, M_{\text{max}}]$, where $M_{\text{max}} = K/2$ for a $K-$channel Kondo model, and $M_{\text{min}} = 0$ if K is even, otherwise $\frac{1}{2}$. Defining $\alpha = \frac{1}{2}\left(\mathcal{J}m + h\right) + \frac{\mathcal{J}}{4}$ and $x_m^M = M(M+1) - m(m+1)$, the partition function can be written as

$$Z(h) = \sum_{M=M_{\text{min}}}^{M_{\text{max}}} r_M^K\Bigg[\sum_{\substack{m=-M,\\ m\in\mathbb{Z}}}^{M-1} 2e^{\beta\frac{\mathcal{J}}{4}}\cosh\beta\sqrt{\mathcal{J}^2 x_m^M/4+\alpha^2} + 2e^{-\beta\mathcal{J}M/2}\cosh\beta h/2\Bigg] . \tag{14}$$

Here, $\beta = \frac{1}{k_BT}$, M sums over the eigenvalues of S while m sums over $\mathcal{J}^z - \frac{1}{2}$ and the additional degeneracy factor $r_M^K = {}^{K-1}C_{K/2-M}$ arises from the possibility that there are multiple subspaces defined by $S = M$. To calculate the impurity magnetic susceptibility, we will use the expression

$$\chi = \frac{1}{\beta}\lim_{h\to 0}\left[\frac{Z''(h)}{Z(h)} - \left(\frac{Z'(h)}{Z(h)}\right)^2\right] . \tag{15}$$

where the $\prime$ indicates derivative with respect to h. For brevity, we define $\theta_M = \beta\mathcal{J}(M+\frac{1}{2})/2$ and $\Sigma_M = \sum_{\substack{m=-M,\\ m\in\mathbb{Z}}}^{M-1}(m+\frac{1}{2})^2$. At low temperatures, the derivatives are

$$Z \to 2r_{M_{\text{max}}}^K M_{\text{max}} e^{\beta\frac{J}{2}(M_{\text{max}}+1)} , \tag{16}$$

$$Z'' \to r_{M_{\text{max}}}^K\left(\frac{\beta}{2(M_{\text{max}}+\frac{1}{2})}\right)^2 e^{\beta\frac{J}{2}(M_{\text{max}}+1)}\Sigma_{M_{\text{max}}} , \tag{17}$$

$$\chi \to \frac{\beta\Sigma_{\text{max}}}{2M_{\text{max}}\left(2M_{\text{max}}+1\right)^2} = \frac{\beta(K-1)}{12(K+1)} \sim \frac{1}{T} . \tag{18}$$

The χ is seen to diverge as T^{-1} at low temperatures. Such a non-analyticity in a response function is a signature of the critical nature of the Hamiltonian. This is in contrast to the behaviour in the non-critical exactly-screened fixed point where the ground state is unique. There, the susceptibility becomes constant at low temperatures: $\chi(T\to 0) = \frac{W}{4T_K}$, T_K being the single-channel Kondo temperature and W the Wilson number

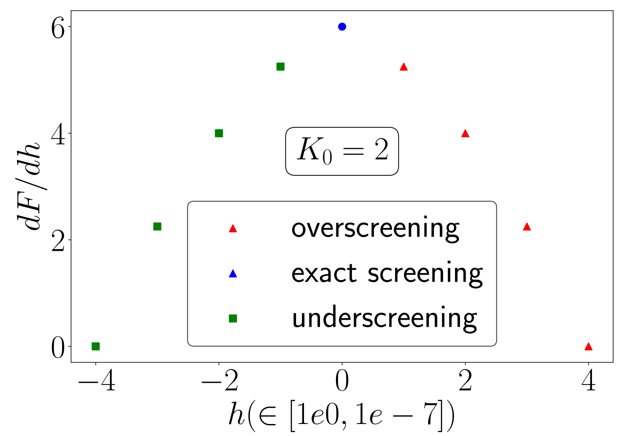

FIG. 3. Variation of the degree of compensation as we tune the system from under-screening to over-screening. The maximum spin compensation occurs at exact-screening $\delta = 0$.

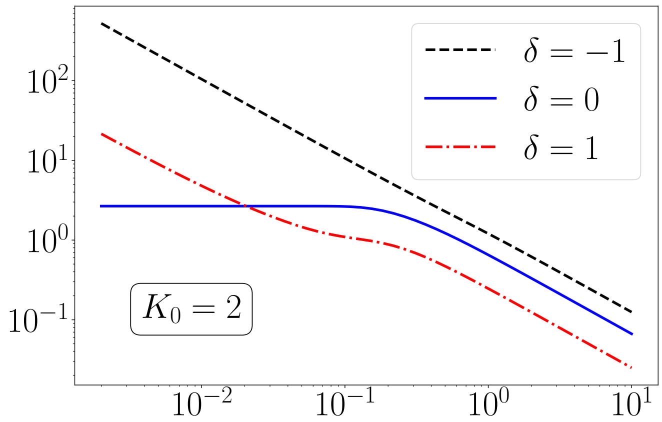

FIG. 4. Variation of impurity susceptibility against temperature. The exactly screened case ($\delta = 0$) saturates to a constant value at low temperatures, indicating complete screening. The cases of inexact screening show a divergence of the susceptibility, which means there is a remnant local spin at the impurity. Since the axes are in log scale, the behaviour is $\log T \sim -\log \chi$ which translates to $\chi \sim 1/T$.

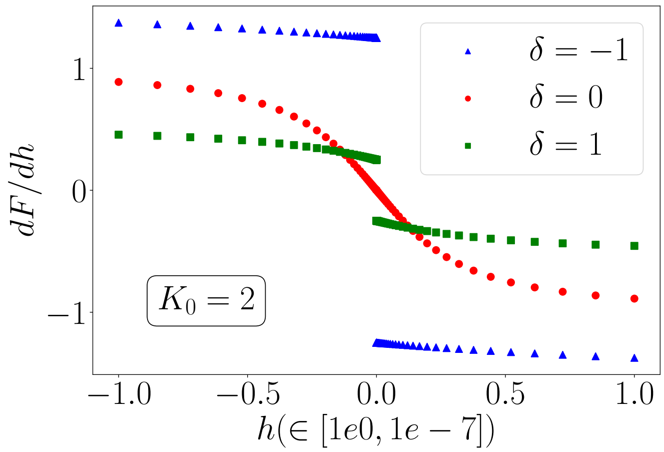

FIG. 5. Behaviour of the impurity magnetization for three values of $(K, 2S) = (2, 4), (3, 3), (4, 2)$. Only the case of $K = 2S = 3\,(\delta = 0)$ is analytic near zero. The non-analyticity of the other cases arises because of the frustration brought about by the degeneracy of the star graph ground state.

[10, 40, 67, 83]. We have checked the case of general spin-S impurity numerically (fig. 4), and the general conclusion is that all exactly-screened models show a constant impurity susceptibility at $T \to 0$, while the over-screened and under-screened cases show a diverging impurity susceptibility in the same limit. A similar divergence is also seen in the susceptibility of the outer spins, calculated by inserting a magnetic field purely on the outer spins.

A second non-analyticity arises when we consider the impurity free energy and the magnetization. The thermal free energy is given by

$$F(h) = -\frac{1}{\beta} \ln Z(h) = -\frac{1}{\beta} \ln \sum_{E_n} e^{-\beta E_n} \ . \tag{19}$$

At $T \to 0$, only the most negative energy E_{min} survives. The minimal energy eigenvalue is

$$E_{\text{min}} = -\frac{J}{4} - \frac{1}{2}\sqrt{J^2(K+1)^2/4 + h^2 + |h|J(K-1)} \ . \tag{20}$$

The first derivative of the free energy with respect to the field gives

$$F'(h \neq 0, T \to 0) = -\frac{2h + J(K-1)\text{sign}(h)}{4\sqrt{\frac{J^2}{4}(K+1)^2 + h^2 + |h|J(K-1)}} \ . \tag{21}$$

There we used the result that the derivative of $|x|$ is $\text{sign}(x)$. If we now take h to zero from both directions, we get the magnetization of the impurity

$$m = F'(h \to 0^{\pm}, T \to 0) = \mp\frac{1}{2}\frac{(K-1)}{(K+1)} \ . \tag{22}$$

The magnetization is therefore discontinuous as $h \to 0$; it goes to different values depending on the direction in which we take the limit. The non-analyticity for $K > 1$ occurs because there is at least one pair of ground state with non-zero parity π^z and magnetic field is able to flip one ground state into the state of opposite parity. This available space for scattering is simply the frustration that we discussed earlier. Indeed, we have checked numerically (see fig. 5) that the non-analyticity exists for all $\delta \neq 0$, where $\delta = \frac{K}{2} - S$ is the deviation from exact screening. Some additional results are presented in the Supplementary Materials [73].

C. Topological properties of ground state manifold

We now present the non-local twist and translation operators which can be used to explore the degenerate ground state manifold of the star graph model. First we define two operators $\hat{T}$ and $\hat{O}$, which we will call the translation and twist operators respectively:

$$\hat{T} \ = \ e^{i\frac{2\pi}{K}\hat{\Sigma}} \ , \ \hat{O} = e^{i\hat{\phi}} \ , \ \ \hat{\Sigma} = [\hat{J}^z - (K-1)/2] \ . \tag{23}$$

One can see that the generators of these above operators commute with the Hamiltonian: $[H, J^x] = [H, J^z] = [H, J^z] = 0$. In the large K limit, we can perform a semi-classical approximation. As J^x and J^y both commute with the Hamiltonian H, we can write $[H, J^y(J^x)^{-1}] = 0$, and any non-singular function of these operators must also commute with the Hamiltonian, which leads us to conclude that

$$\hat{\phi} = \tan^{-1}(\hat{J}^y(\hat{J}^x)^{-1}) \ . \tag{24}$$

We then get $[\hat{\phi}, \hat{H}] = 0$. We can label the ground states by the eigenvalues of the translation operator $\hat{T}$. We can also use the ground states labeled by the eigenvalues of

J^z (say M). The ground states are now written as

$$|M_1\rangle, |M_2\rangle, |M_2\rangle, \cdots, |M_K\rangle \ . \tag{25}$$

The operations of the translation operators on this states are then given by

$$\hat{T}|M_i\rangle = e^{i\frac{2\pi}{K}[M_i-(K-1)/2]}|M_i\rangle = e^{i2\pi\frac{p_i}{K}}|M_i\rangle \ , \ p_i \in [K] \ . \tag{26}$$

The braiding rule between the twist and the translation operators is

$$\begin{aligned} \hat{T}\hat{O}\hat{T}^\dagger\hat{O}^\dagger &= e^{\frac{2\pi}{K}[i\hat{\Sigma}, i\hat{\phi}]} = e^{i\frac{2\pi}{K}} \ , \\ \hat{T}\hat{O}^m\hat{T}^\dagger\hat{O}^{\dagger m} &= e^{\frac{2\pi}{K}[i\hat{\Sigma}, im\hat{\phi}]} = e^{i2\pi\frac{m}{K}} \ . \end{aligned} \tag{27}$$

Next, we shown that the states $\hat{O}^m|M_i\rangle$ are orthogonal to each other and with the state $|M_i\rangle$.

$$\hat{T}\hat{O}^m|M_i\rangle = \hat{O}^m\hat{T}e^{i2\pi\frac{m}{K}}|M_i\rangle = \hat{O}^m e^{i\frac{2\pi(m+p_i)}{K}}|M_i\rangle \tag{28}$$

$$\hat{T}\bigg(\hat{O}^m|M_i\rangle\bigg) = e^{i\frac{2\pi(m+p_i)}{K}}\bigg(\hat{O}^m|M_i\rangle\bigg) \tag{29}$$

Different states $\hat{O}^m|M_i\rangle$ for different m are therefore labeled by different eigenvalues of the translation operations, and are thus orthogonal to each other. As the twist operator $\hat{O}$ commutes with the Hamiltonian, we can write

$$\langle M_i|\hat{O}^{m\dagger}H\hat{O}^m|M_i\rangle = \langle M_i|H|M_i\rangle \ . \tag{30}$$

Thus the energy eigenvalues of all the orthogonal states are equal, and they form the K fold degenerate ground state subspace. By the application of the twist operator $\hat{O}$, one can go from one degenerate ground state to another.

D. Local Mott liquid

By applying the unitary renormalization group method on the zero mode star graph Hamiltonian, we decouple the impurity spin from the zero-modes of the K channels:

$$\begin{aligned} H &= \mathcal{J}\vec{S}_d.\sum_i \vec{S}_i = \mathcal{J}S_d^z S^z + \frac{\mathcal{J}}{2}(S_d^+S^- + S_d^-S^+) \ , \\ H_D &= \mathcal{J}S_d^z S^z \ , \quad H_X = \frac{\mathcal{J}}{2}(S_d^+S^- + S_d^-S^+) \ . \end{aligned} \tag{31}$$

In order to remove the quantum fluctuations between the impurity spin and the rest, we perform one step of URG:

$$\Delta H \ = \ H_X(\hat{\omega} - H_D)^{-1}H_X \tag{32}$$

The total bath spin operator S^z is not a good quantum number for the zero mode ground state, and because there is no net S^z field, the ground state manifold has a vanishing expectation value of S^z, $\langle S^z\rangle = 0$. We use this expectation value to replace the denominator of the above RG equation.

$$\beta_\uparrow(\mathcal{J}, \omega_\uparrow) = (\mathcal{J}^2\Gamma_\uparrow)/2 \ , \ \ \Gamma_\uparrow = (\omega_\uparrow - \mathcal{J}(S_d^z - 1))^{-1} \ . \tag{33}$$

The effective Hamiltonian is therefore

$$H_{eff} = \frac{\beta_\uparrow(\mathcal{J}, \omega_\uparrow)}{4}(S^+S^- + S^-S^+) \ . \tag{34}$$

In terms of the electronics degree of freedom, it has the form

$$\frac{\beta_\uparrow(\mathcal{J}, \omega_\uparrow)}{4}\sum_{\substack{i\neq j \\ \alpha_i,\beta_i\in\{\uparrow,\downarrow\} \\ \alpha_j,\beta_j\in\{\uparrow,\downarrow\}}} \vec{\sigma}_{\alpha_i\beta_i}\vec{\sigma}_{\alpha_j\beta_j}c^{(i)\dagger}_{0\alpha_i}c^{(i)}_{0\beta_i}c^{(j)\dagger}_{0\alpha_j}c^{(j)}_{0\beta_j} + \text{h.c.} \ . \tag{35}$$

The antiferromagnetic case is for $\frac{\beta_\uparrow(\mathcal{J},\omega_\uparrow)}{2} < 0$. In this case, the ground state is realised for S being maximum and S^z being minimum. The effective Hamiltonian can be rewritten in this case as

$$H_{eff} = -|\beta_\uparrow(\mathcal{J}, \omega_\uparrow)| \times (S^+S^- + S^-S^+)/4 \ . \tag{36}$$

The complete set of commuting observables for this Hamiltonian contains H, S, S^z. In the ground state, S is maximum, and therefore $S = K/2$, and S^z can take $2S + 1 = K + 1$ values. In the largest S sector there are $K + 1$ states. Defining the dual operator $\hat{\phi}$ with the algebra $[\phi, \hat{S^z}] = i$, we get the twist operator $\hat{Q} = \exp(i\hat{\phi}\Phi/\Phi_0)$. Applying this operator, we get the twisted Hamiltonian

$$H(\Phi) = -\frac{|\beta_\uparrow(\mathcal{J}, \omega_\uparrow)|}{2}S^2 + \frac{|\beta_\uparrow(\mathcal{J}, \omega_\uparrow)|}{2}\bigg(S^z - \frac{\Phi}{\Phi_0}\bigg)^2 \ . \tag{37}$$

One can thus explore different S^z ground states via such flux tuning mechanism.

For a K channel star graph problem the ground state is K fold degenerate associated with different J^z values $\{-(K-1)/2, -(K-3)/2, \cdots, (K-1)/2\}$. After removing the quantum fluctuations between the impurity spin and the outer spins, we get an all-to-all model (eq.(37)) as the effective Hamiltonian. The eigenstates of this all-to-all Hamiltonian can be labeled by the eigenvalues of S^z. There are $K + 1$ such states made out of only the outer spins. The total state including the impurity spin can be written as $|J^z\rangle = |S_d^z\rangle\otimes|S^z\rangle$ labeled by $J^z = S_d^z + S^z$. As the all-to-all model has Z_2 symmetry in impurity sector, there are $2(K + 1)$ total states. For $S_d^z = 1/2$, $\{J^z\} = \{-(K-1)/2, \cdots, (K-1)/2, (K+1)/2\}$ and for $S_d^z = -1/2$, $\{J^z\} = \{-(K+1)/2, -(K-1)/2, \cdots, (K-1)/2\}$. We can see that in both the cases, all K states of the star graph ground state manifold are present in the spectrum of the all-to-all model, one of them being the ground state. Using the twist operator, we can cycle between the various states. Some additional topological features of the Mott liquid are presented in the Supplementary Materials [73].

IV. LOCAL NON-FERMI LIQUID EXCITATIONS OF THE 2CK MODEL

A. Effective Hamiltonian

We will now proceed to extract the nature of the low-energy excitations of the two-channel Kondo problem. This will be done by adding real-space hopping to the zero-bandwidth Hamiltonian and treating this hopping as a perturbation above the zero-bandwidth Hamiltonian. The zero-bandwidth Hamiltonian obtained from the URG of the two-channel Kondo problem then acts as the zeroth-level Hamiltonian Here:

$$H^{(2)} \;=\; \mathcal{J}\vec{S}_d.(\vec{S}_1+\vec{S}_2) \quad , \quad \vec{S}_i = \frac{1}{2}\; c^\dagger_{i,\alpha}\; \vec{\sigma}_{\alpha,\beta}\; c_{i,\beta} \quad (38)$$

Here, $\vec{S}_i = 1,2$ represents the spin degree of freedom present at the origin of the i^{th} channel. This zeroth-level Hamiltonian has two degenerate ground states labeled by $|J^z = \pm 1/2\rangle$ with energy $-\mathcal{J}$ and 6 excited states [96]. The perturbation Hamiltonian is the real-space hopping:

$$H_X \;=\; -t \sum_{\substack{<1,l_1> \\ <2,l_2>}} (c^\dagger_{1,\sigma}c_{l_1,\sigma} + c^\dagger_{2,\sigma}c_{l_2,\sigma} + \text{ h.c.}) \;, \quad (39)$$

and it will be accounted for using degenerate perturbation theory. Here l_i represents the nearest site to the origin of the i^{th} channel.

Since the perturbation is a single-particle hopping that transfers electrons, we need to rewrite the spin operators in the zeroth Hamiltonian in terms of fermionic operators:

$$\mathcal{H} \;=\; \frac{\mathcal{J}\hbar}{2}\; \vec{S}_d. \sum_{i=\{1,2\}} \sum_{\alpha,\beta\in\{\uparrow,\downarrow\}} c^\dagger_{i\alpha}\vec{\sigma}_{\alpha\beta}c_{i\beta} + H_X \;. \quad (40)$$

In this expanded basis, there are 32 degenerate ground states:

$$\{|\alpha_i\rangle\} = \{|J^z\rangle \otimes |n_{l_1,\uparrow}, n_{l_1,\downarrow}, n_{l_2,\uparrow}, n_{l_2,\downarrow}\rangle\} \;. \quad (41)$$

The $32-$fold degeneracy arises from the two-fold degeneracy of J^z ($J^z = \pm 1/2$) multiplying the $16-$fold degeneracy of the rest of the sites $n_{l_i,\sigma}$ (each of the four $n_{l_i,\sigma}$ can be 0 or 1, leading to a 2^4-fold degeneracy).

The first and the second order corrections to the low energy effective Hamiltonian are

$$H^{(1)} \;=\; \sum_{ij} |\alpha_i\rangle\langle\alpha_i|V|\alpha_j\rangle\langle\alpha_j| \;.$$
$$H^{(2)} \;=\; \sum_{ij}\sum_{l} |\alpha_i\rangle \frac{\langle\alpha_i|V|\mu_l\rangle\langle\mu_l|V|\alpha_j\rangle}{E_0 - E_l}\langle\alpha_j| \;. \quad (42)$$

Here, $|\alpha_i\rangle$ represents the ground states with energy E_0 and is the set of states defined in eq. 41, and μ_l represents the excited states with energy E_l. It is easy to see that the diagonal contribution at any odd order is zero - the final state is never equal to the initial state. The off-diagonal part at first order is also zero. At second order we get both diagonal and off-diagonal contributions to the effective Hamiltonian.

1. Diagonal renormalisation

We first calculate the diagonal renormalisation at second order coming from each of the states $|\tilde{\alpha}_0\rangle = |J^z = \frac{1}{2}\rangle \otimes |\psi_{\text{rest}}\rangle \,, |\tilde{\alpha}_1\rangle = |J^z = -\frac{1}{2}\rangle \otimes |\psi_{\text{rest}}\rangle$, where $|\psi_{\text{rest}}\rangle$ refers to the configuration of the remaining sites apart from the two that form the zeroth Hamiltonian. These second order corrections are given by

$$H^{(2)}_{\text{diag}}(\tilde{\alpha}_0) = \frac{2t^2}{E_0}\hat{I} - \Omega_l, \quad H^{(2)}_{\text{diag}}(\tilde{\alpha}_1) = \frac{2t^2}{E_0}\hat{I} + \Omega_l \;, \quad (43)$$

where $S^z_{l_i} = (n_{l_i\uparrow} - n_{l_i\downarrow})/2$ and $\Omega_l = \frac{2t^2}{3E_0}(S^z_{l_1} + S^z_{l_2})$. The total diagonal second-order contribution to the effective Hamiltonian is obtained by adding these two contributions, and the result is a trivial shift: $H^{(2)}_{\text{diag}} = H^{(2)}_{\text{diag}}(\tilde{\alpha}_0) + H^{(2)}_{\text{diag}}(\tilde{\alpha}_1) = -4t^2\hat{I}$. The fact there is no non-trivial diagonal renormalisation to the low-energy excitations shows the absence of (local) Fermi liquid terms, and this occurs because of the exact cancellation of the field terms $\pm\Omega_l$.

2. Off-diagonal renormalisation

The off-diagonal contribution to the second order effective Hamiltonian is

$$\begin{aligned} H_{NFL} \;&=\; H^{(2)}_{off} = \sum_{i\neq j}\sum_{l} |\alpha_i\rangle \frac{\langle\alpha_i|V|\mu_l\rangle\langle\mu_l|V|\alpha_j\rangle}{E_0 - E_l}\langle\alpha_j| \\ &=\; -\frac{8t^2}{3}[(S^z_1)^2 c^\dagger_{2\uparrow}c_{2\downarrow}(c_{l_1\uparrow}c^\dagger_{l_1\downarrow} + c_{l_2\uparrow}c^\dagger_{l_2\downarrow}) \\ &+\; (S^z_2)^2 c^\dagger_{1\uparrow}c_{1\downarrow}(c_{l_1\uparrow}c^\dagger_{l_1\downarrow} + c_{l_2\uparrow}c^\dagger_{l_2\downarrow})] + \text{h.c.} \;. \quad (44) \end{aligned}$$

This effective Hamiltonian is purely of the non-Fermi liquid kind, arising due to the degeneracy of the ground state manifold. Using this low energy effective Hamiltonian we have calculated different thermodynamic quantities like susceptibility, specific heat and the Wilson ratio. The first two measures show logarithmic behavior at low temperatures, in agreement with known results in the literature. These results are shown in the Supplementary Material [73].

Following this method, we have also calculated the effective Hamiltonian for the three channel Kondo model. We again find the absence of all Fermi liquid terms up to 2^{nd} order, and the presence of non-Fermi liquid terms in the off-diagonal part of the effective Hamiltonian, and these are also shown in the Supplementary Material [73].

B. Local marginal Fermi liquid and orthogonality catastrophe

The real space local low energy Hamiltonian that takes into account the excitations above the ground state is given by eq. 44 and can be written as

$$V_{\text{eff}} = \frac{2t^2}{\mathcal{J}^*}\left[\left(\sigma^z_{0,1}\right)^2 s^+_{0,2} + \left(\sigma^z_{0,2}\right)^2 s^+_{0,1}\right]\left(s^-_{1,1} + s^-_{1,2}\right) + \text{h.c.}\ ; \tag{45}$$

here, $\sigma^z_{0,l} = \hat{n}_{0\uparrow,l} - \hat{n}_{0\downarrow,l}, s^+ = c^\dagger_{0\uparrow,l}c_{0\downarrow,l}$ and $s^- = (s^+)^\dagger$. The notation $0\sigma, l$ has the site index $i = 0, 1, 2, \ldots$ as the first label, the spin index $\sigma =\uparrow,\downarrow$ as the second label and the channel index $l = 1, 2$ as the third index. Such non-Fermi liquid (NFL) terms in the effective Hamiltonian and the absence of any Fermi-liquid term at the same order should be contrasted with the local Fermi liquid excitations induced by the singlet ground state of the single-channel Kondo model [1, 10, 83]. We now take the MCK Hamiltonian to strong-coupling, and perform a perturbative treatment of the hopping. At $J \to \infty$, the perturbative coupling t^2/J is arbitrarily small and we again obtain Eq. 45. Such a change from the strong coupling model with parameter J to a weak coupling model with parameter t^2/J amounts to a duality transformation [85, 86]. It can be shown that the duality transformation leads to an identical MCK model [85] (self-duality), which implies we can have identical RG flows, and our transformation simply extracts the NFL piece from the dual model. The self-duality also ensures that the critical intermediate-coupling fixed point is unique and can be reached from either of the models.

The diagonal part of eq. 45 is

$$V_{\text{eff}} = \frac{2t^2}{J}\sum_{l=1,2}\left(\sum_\sigma \hat{n}_{0\sigma,l}\right) s^+_{0,\bar{l}}s^-_{1,\bar{l}} + \text{h.c.}\ , \tag{46}$$

where $\bar{l} = 3 - l$ is the channel index complementary to l. We will Fourier transform this effective Hamiltonian into $k-$space. The NFL part becomes

$$\sum_{\sigma,\left\{k_i,k_i'\right\},l} \frac{2t^2}{J} e^{i\left(k_1-k_1'\right)a} c^\dagger_{k\sigma,l}c_{k'\sigma,l}c^\dagger_{k_2\uparrow,\bar{l}}c_{k_2'\downarrow,\bar{l}}c^\dagger_{k_1\downarrow,\bar{l}}c_{k_1'\uparrow,\bar{l}} + \text{h.c.}\ . \tag{47}$$

This form of the Hamiltonian is very similar to the three-particle interaction term in Appendix B of [70]. The channel indices in Eq. 47 can be mapped to the normal directions in [70]. The 2 particle-1 hole interaction in Eq. 47 has a diagonal component which can be obtained by setting $k = k', k_1 = k_2'$ and $k_2 = k_1'$:

$$\begin{aligned} H_{\text{eff,MFL}} &= \sum_{\substack{k,k_1,\\k_2,\sigma,l}} \frac{2t^2 e^{i(k_1-k_2)a}}{J}\hat{n}_{k\sigma,l}\hat{n}_{k_2\uparrow,\bar{l}}\left(1 - \hat{n}_{k_1\downarrow,\bar{l}}\right) + \text{h.c.} \\ &= \sum_{\substack{k,k_1,\\k_2,\sigma,l}} \frac{4t^2}{J}\cos a\left(k_1 - k_2\right)\hat{n}_{k\sigma,l}\hat{n}_{k_2\uparrow,\bar{l}}\left(1 - \hat{n}_{k_1\downarrow,\bar{l}}\right)\ . \end{aligned} \tag{48}$$

The most dominant contribution comes from $k_1 = k_2 = k'$, revealing the non-Fermi liquid metal [45, 91]:

$$H^*_{\text{eff,MFL}} = \frac{4t^2}{J}\sum_{\sigma,k,k',l}\hat{n}_{k\sigma,l}\hat{n}_{k'\uparrow,\bar{l}}\left(1 - \hat{n}_{k'\downarrow,\bar{l}}\right)\ . \tag{49}$$

A non-local version of this effective Hamiltonian was found to describe the normal phase of the Mott insulator of the 2D Hubbard model, as seen from a URG analysis [70, 71]. Following [70], one can track the RG evolution of the dual coupling $R_j = \frac{4t^2}{J_j}$ at the j^{rh} RG step, in the form of the URG equation

$$\Delta R_j = -\frac{R_j^2}{\omega - \epsilon_j/2 - R_j/8}\ . \tag{50}$$

In the RG equation, ϵ_j represents the energy of the j^{th} isoenergetic shell. It is seen from the RG equation that R is relevant in the range of $\omega < \frac{1}{2}\epsilon_j$ that has been used throughout, leading to a fixed-point at $R^*/8 = \omega - \frac{1}{2}\epsilon^*)$. The relevance of R is expected because the strong coupling J is irrelevant and $R \sim 1/J$.

The renormalisation in R leads to a renormalisation in the single-particle self-energy [70]. The $k-$space-averaged self-energy renormalisation is

$$\Delta\Sigma(\omega) = \rho {R^*}^2\int_0^{\epsilon^*}\frac{d\epsilon_j}{\omega - \epsilon_j/2 + R_j/8}\ . \tag{51}$$

The density of states can be approximated to be N^*/R^*, where N^* is the total number of states over the interval R^*. As suggested by the fixed point value of R_j, we can approximate its behaviour near the fixed point by a linear dependence of the dispersion ϵ_j. The two limits of the integration are the start and end points of the RG. We start the RG very close to the Fermi surface and move towards the fixed point ϵ^*. Near the start point, we substitute $\epsilon = 0$ and $R = \omega$, following the fixed point condition. From the fixed point condition, we also substitute $R^*/8 = \omega - \frac{1}{2}\epsilon^*$. On defining $\bar{\omega} = N^*\left(\omega - \frac{1}{2}\epsilon^*\right)$, we can write

$$\Delta\Sigma(\omega) \sim \bar{\omega}\ln\frac{N^*\omega}{\bar{\omega}}\ . \tag{52}$$

The self-energy also provides the quasiparticle residue for each channel[70]:

$$Z(\bar{\omega}) = \left(2 - \ln\frac{2\bar{\omega}}{N^*\omega}\right)^{-1}\ . \tag{53}$$

As $\omega \to 0$, the Z vanishes, implying that the ground state is not adiabatically connected to the Fermi gas in the presence of the NFL terms. This is the orthogonality catastrophe [97–100] in the two-channel Kondo problem, and it is brought about by the presence of the channel-non diagonal terms in Eq. 49. Such terms were absent in the single-channel Kondo model, because there was no multiply-degenerate ground state manifold that allowed scattering. This line of argument shows that the extra degeneracy of the ground state subspace and the frustration of the singlet order that comes about when one upgrades from the single-channel Kondo model to the MCK models is at the heart of the NFL behaviour, and the orthogonality catastrophe is expected to be a general feature of all such frustrated MCK models. A local NFL term and a similar self-energy was also obtained by Coleman, et al. [49] in terms of Majorana fermions at the strong-coupling fixed point of the $\sigma-\tau$ model, which they claimed was equivalent to the intermediate-coupling fixed point of the two-channel Kondo model. Along with the work by Schofield [39], this demonstration shows the universality between the two-channel Kondo and the $\sigma-\tau$ models.

V. ENTANGLEMENT PROPERTIES

A. Entanglement properties of the star graph

We will now present the results of our study of various entanglement measures in each of the K degenerate ground states $|J^z\rangle$ of a K channel star graph, labeled by the eigenvalues of J^z.

1. *Entanglement entropy between impurity and the rest*

In a 1-channel Kondo model, the ground state is unique and a singlet [83]: $|J, J_z = 0, 0\rangle = \frac{1}{\sqrt{2}}\left(|\uparrow_d, \downarrow_0\rangle - |\downarrow_d, \uparrow_0\rangle\right)$, and the impurity entanglement entropy (EE_d) is at the maximum possible value of $\log 2$. We will now calculate the same quantity for the ground states

$$|J^z\rangle \equiv |S_d = 1/2, S = K/2; J = (S-1/2), J^z\rangle \tag{54}$$

of the K channel model.

In order to compute EE_d for a particular state $|J^z\rangle$, we calculate the von-Neumann entropy of the reduced density matrix ρ_d obtained by partially tracing the density matrix $\rho = |J^z\rangle\langle J^z|$ associated with the state $|J^z\rangle$ over the impurity states $|S^z_d = \pm\frac{1}{2}\rangle$:

$$\rho_d = \mathrm{Tr}_d \rho = \sum_{S^z_d} \langle S^z_d|\rho|S^z_d\rangle\ , \quad EE_d = -\rho_d \log \rho_d \tag{55}$$

The EE_d for states of various J^z are shown as functions of the number of channels K in fig. 6. At any given value of K on the $x-$axis, all the points directly above it represent values of EE_d for various values of J^z in the ground state manifold of the MCK problem defined by that particular value of K. The minimum entanglement entropy occurs in the maximum J^z state ($|J^z = J\rangle$), and this minimum value decreases with increase in K. On the other hand, the maximum entanglement entropy is attained in the state with minimum J^z. This maximum value of the entanglement entropy is always $\ln 2$ for odd values of K; for even values of K, the value asymptotically reaches $\log 2$ at large K.

A very similar computation gives the entanglement entropy between one outer spin and the rest of the spins, and it is shown in Fig. 7. We again find that the minimum entanglement entropy is associated with the state

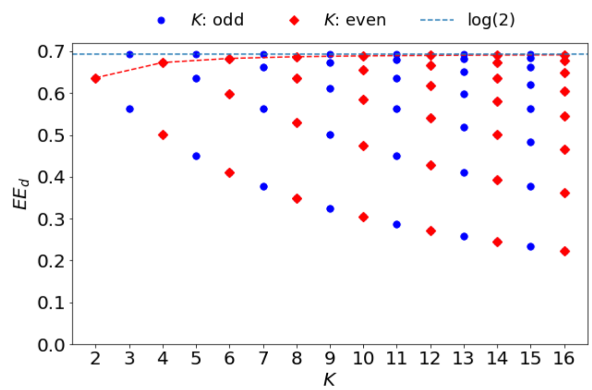

FIG. 6. Variation of impurity entanglement entropy (EE_d) for multiple values of K. The maximum EE_d at large K is $\log 2$.

$|J^z = J\rangle$ and it falls with increasing K, approaching zero asymptotically; the maximum entanglement entropy is, as before, associated with the state $|\,(J^z)_{\text{min}}\rangle$ and it rises to $\log 2$ in the limit $K \gg 1$.

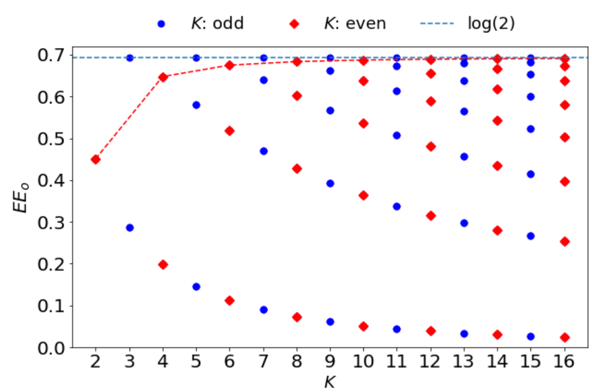

FIG. 7. Variation of the entanglement entropy of an outer spin (EE_o) with the rest for different channels (K). The maximum entanglement entropy in the large K limit is $\log 2$.

Two interesting features emerge from the study:

- For the odd K models, the impurity is maximally entangled with the other spins in the minimum J^z, $|J^z = 0\rangle$, member of the ground state manifold. At large K, the even K models also acquire this property, the minimum J^z there being $\pm\frac{1}{2}$.

- Both EE_d and EE_0 are individually equal for the states $|\pm J^z\rangle$, which shows that both types of entanglement entropy are invariant under the transformation $|J^z\rangle \to \pi\,|J^z\rangle$. This reflects a parity symmetry in the state space in terms of entanglement.

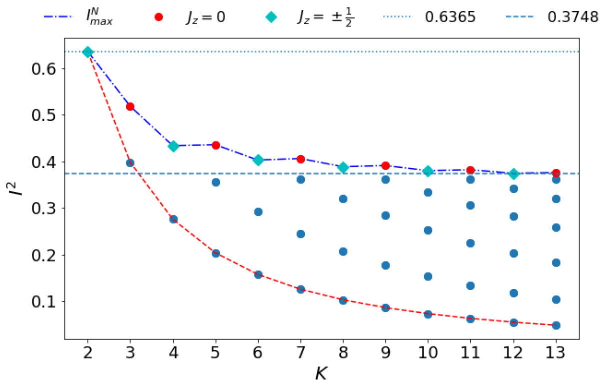

FIG. 8. Variation of mutual information $I^2(d:o)$ of the impurity with the rest, for different values of K. The maximum $I^2(d:o)$ is 0.37.

2. Mutual Information

Mutual information is a measure which captures the correlations present between two subsystems (A,B), in a particular state. It is defined as

$$I^2(A:B) = S_A + S_B - S_{A\cup B} \ , \tag{56}$$

where $S_{A(B)}$ is the von-Neumann entanglement entropy of the subsystem $A(B)$ with the rest, and $S_{A\cup B}$ is the von-Neumann entanglement entropy of A and B with the rest. We are interested in two types of mutual information: firstly, the mutual information $I^2(d:o)$ between the impurity and one of the other spins, and secondly, the mutual information $I^2(o:o)$ between any two of the outer spins. Both of these have been computed for various channel numbers K, and plotted in Figs. 8 and 9.

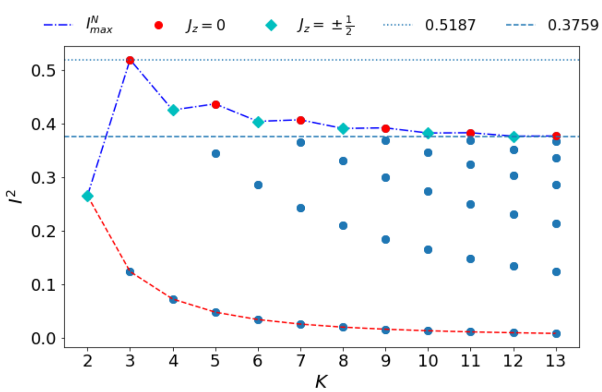

FIG. 9. Variation of mutual information $I^2(o:o)$ between 2 outer spins, for multiple K. $I^2(o:o)$ vanishes for large K.

In both cases we find that the maximum and minimum mutual information are associated with the $|\,(J^z)_{\min}\rangle$ and $|J^z = J\rangle$ states respectively. We also find that the mutual information is the same in the states $|J^z\rangle$ and $\pi^x|J^z\rangle$, indicating the parity symmetry in the mutual information

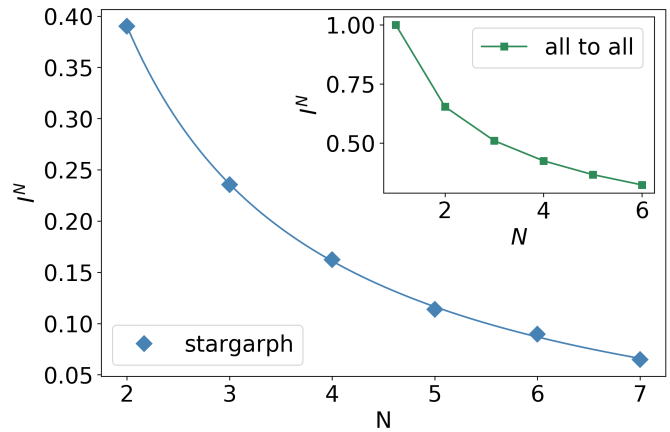

FIG. 10. Variation of multipartite information I^N among N outer spins as a function of N, for $K = 8$. The inset shows I^N vs N for an all-to-all model. Both show power law behavior.

measure. In the large channel limit ($K \gg 1$), the maximum $I^2(d:o)$ and $I^2(o:o)$ saturate to the common value of 0.375.

3. Multipartite information

Similar to mutual information, one can calculate higher order multipartite information to study the nature of correlations present in different ground states. We define the tripartite information among three subsystems A, B, C as $I^3_{ABC} = (S_A + S_B + S_C) - (S_{AB} + S_{BC} + S_{CA}) + S_{ABC}$. I^3 shows behavior similar to the mutual information - the highest I^2 value is associated with the $(J^z)_{\min}$ state and it saturates in the limit of $K \gg 1$. One can measure $N-$partite information for a collection of subsystems (CSS) $\{\mathcal{A}_N\} \equiv \{A_1, A_2, \cdots, A_N\}$. To define the $N-$partite information, we first define the power set of the CSS $\{\mathcal{A}_N\}$ as $\mathcal{P}(\{\mathcal{A}_N\})$, and the collection of all subsets of $\mathcal{P}(\{\mathcal{A}_N\})$ with m subsystems in it as $\mathcal{B}_m(\{\mathcal{A}_N\}) \equiv \{Q \mid Q \subset \mathcal{P}(\{\mathcal{A}_N\}), |Q| = m\}$. We also define the union and intersection of all the subsystems present in Q as $V_\cup(Q) \equiv \bigcup_{A\in Q} A$ and $V_\cap(Q) \equiv \bigcap_{A\in Q} A$ respectively. Then, the $N-$partite information that we are interested in is defined as

$$I^N_{\{\mathcal{A}_N\}} = \left[\sum_{m=1}^{N}(-1)^{m-1}\sum_{Q\in\mathcal{B}_m(\{\mathcal{A}\})} S_{V_\cup(Q)}\right] - S_{V_\cap(\mathcal{A}_N)} \ . \tag{57}$$

The study of such measures of multipartite information reveals the nature of the multi-party correlations present among the outer spins of the star graph. Our study, as presented in fig. (10), shows that the higher order multipartite correlations (I^N) decrease as you increase the order (N), and the behaviour follows a power law. In the inset of the same figure, we have shown the I^N vs N plot that is observed in the ground state of the all-to-all effective Hamiltonian (Eq.37), and it shows a similar power-law behaviour. The similarities in the behavior suggest that one can capture entanglement properties either from the star graph or from the corresponding all-to-all model.

B. Entanglement properties at the fixed point of the MCK model

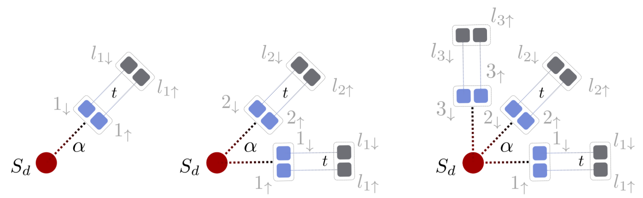

FIG. 11. This is a schematic diagram of (a) single channel and (b) two channel problem. S_d is the impurity spin. For more details refer to the text.

To study the nature of correlations at the MCK fixed point, we introduce excitations into the star graph ground state. We will work with the Hamiltonian Eq.(40) where we consider nearest-neighbor real space hopping t from the zeroth site into the lattice (Fig. 11). Setting $t = 0$ recovers the zero bandwidth version of the MCK. In the $K = 1$ single channel case, the impurity (S_d) is coupled to the spin degree of freedom at the real space origin ($\{1_\uparrow, 1_\downarrow\}$) of the single conduction bath via a Heisenberg spin-exchange coupling. For $K = 2$, the impurity is interacting with 2 distinct local spins $\{1_\uparrow, 1_\downarrow\}$ and $\{2_\uparrow, 2_\downarrow\}$ belonging to zeroth sites of different conduction channels, and the real space hopping connects these zeroth sites to their nearest neighbor sites. As we increase the hopping strength t from zero to non-zero, the lattice sites start interacting with each other.

1. *Impurity entanglement entropy*

The impurity entanglement entropy $EE_d(t)$ in the ground state is shown as a function of t in Fig. 12 for three values of channel number K. At low hopping strength ($0 < t \ll 1$), EE_d is independent of t and achieves a constant value. This value decreases with increasing K. We also find that in this range of t, EE_d decreases with increasing K. This behaviour is reversed at high t, and EE_d is seen to increase with increasing K. Though the values of the impurity entanglement entropy for various values of K are quite similar at low hopping strength, there is a difference in the behaviour as a function of t: the single channel EE_d varies smoothly at $t \to 0^+$, whereas the EE_d for $K > 1$ show a discontinuity at $t \to 0^+$.

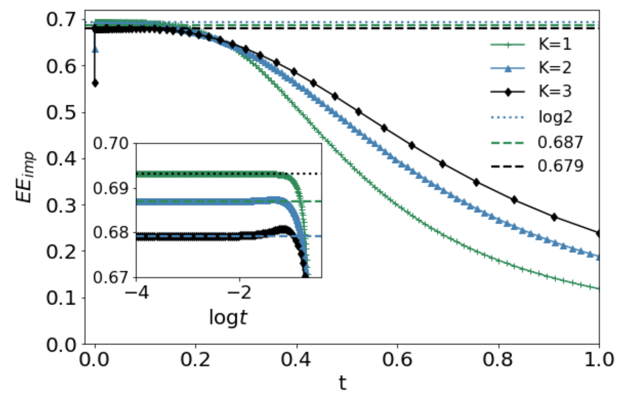

FIG. 12. Variation of impurity entanglement entropy EE_{imp} against t, for $K = 1, 2, 3$.

2. *Intra-channel Mutual information*

Here, we will calculate the mutual information between two electronic states in the ground state wavefunction, as a function of the hopping strength t.

Case 1: We first study the mutual information $MI(d, 1\uparrow)$ between the impurity spin S_d and the state $1_\uparrow$ (fig. 11), where 1 represents real-space origin of the 1^{st} conduction channel. For a single channel model, this site is unique because there is just one channel, but in the presence of K channel, there are K possible choices corresponding to each of the channels. However, because of the symmetry of the Hamiltonian under the exchange of the channel indices, all such choices will show identical mutual information signatures. Similarly, due to the $SU(2)$ spin-rotation symmetry of the Hamiltonian, $MI(d, 1\downarrow)$ will be identical to $MI(d, 1\uparrow)$. We have numerically computed and plotted $MI(d, 1\uparrow)$ as a function of t in fig. 13. The inset shows that at low hopping strength, the mutual information for the single channel and the two-channel models saturate to different values. In the single-channel case, the saturation value at $t = 0$ is $\log 2$, and the mutual information changes smoothly as t is turned on. This is similar to the behaviour in the impurity entanglement entropy studied previously. The value of $\log 2$ shows the maximal entanglement between the zeroth site and the impurity, and the perfect screening of the impurity spin. For the two channel problem, we find that the mutual information at $t = 0$ is $MI(d, 1_\uparrow) = 0.2401$. The reduction of the value from $\ln 2$ shows the breakdown of screening. Also note that unlike the single channel case, there is a discontinuity in $MI(d, 1_\uparrow)$ as t is increased from 0.

Case 2: We have also computed the mutual information $MI(1_\uparrow, 1_\downarrow)$ between the two electronic states on the zeroth site of the same conduction channel, and plotted them in fig. 14. We find that it is a smooth function of t for $K = 1$, and for $K = 2$ there is a discontinuity at $t = 0^+$. Note that for small values of t, we find

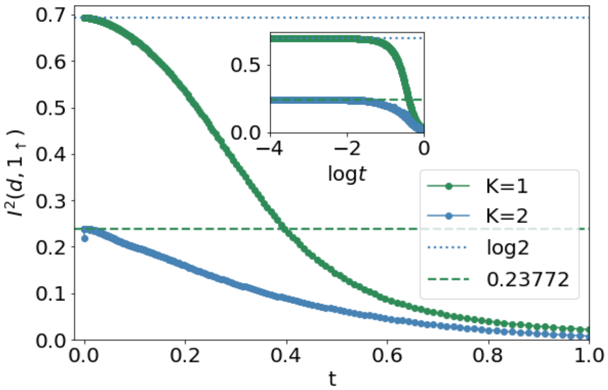

FIG. 13. This figure show the variation of mutual information between the impurity spin and the $1_{\uparrow}$ state against t. For more details please refer to the text. The error-bar σ_2 of the two channel data at low hopping strength $\sigma_2 \approx 0.002$.

$MI(1_{\uparrow}, 1_{\downarrow}) > MI(d, 1_{\uparrow})$ for the $K = 2$ model, showing the presence of strong intra-site correlations.

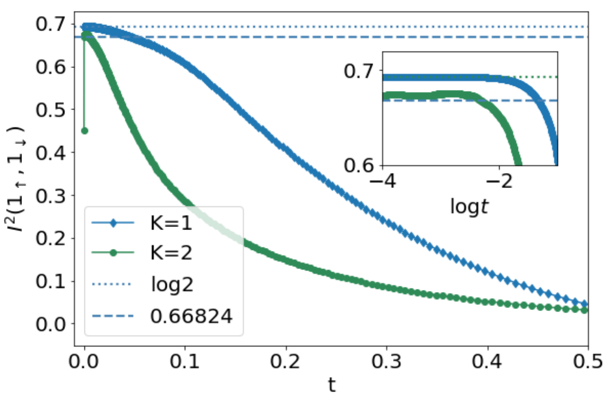

FIG. 14. Variation of mutual information $(i^2(1_{\uparrow}, 1_{\downarrow}))$ among the two states present on the real-space origin (1) of a conduction channel, against t. The error-bar σ_2 for the two channel at low hopping strength is $\sigma_2 \approx 0.013$.

Case 3: Next, we measure the mutual information $MI(d, l_{1\uparrow})$ between the impurity site and an electronic state of site that is nearest-neighbour to the real-space origin of one of the conduction channels (see fig. 11). The results are shown in fig. 15. Vanishing mutual information for the single channel case shows the perfect screening of the impurity spin. The non-zero value of mutual information at small t values in the $K = 2$ model is again a result of the imperfect screening. As in the previous cases, we find a discontinuity in the mutual information for $K = 2$ as $t \rightarrow= 0^{+}$.

Case 4: A complementary study can be made by calculating the mutual information between the origin of a particular conduction channel and it's nearest neighbour

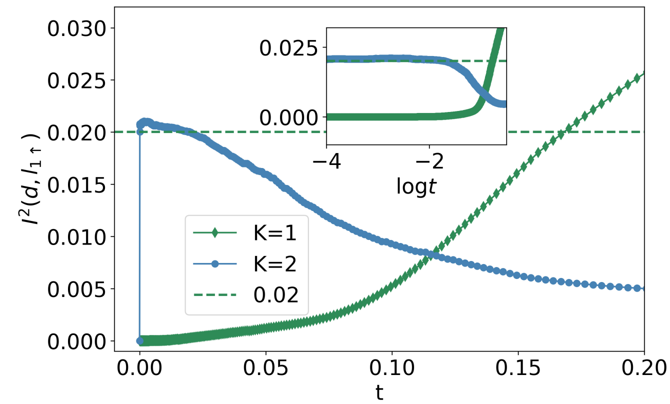

FIG. 15. Variation of the mutual information $MI(d, l_{1\uparrow})$ between the impurity spin and the $l_{1\uparrow}$ state, against t. The error-bar σ_2 for the two channel case is $\sigma_2 \approx 0.001$.

site. They are plotted in fig. 16, and we find that at low hopping strength the single channel mutual information vanishes, showing the decoupling of those two states. On the other hand, in the two channel case, there is a non-zero mutual information which indicates the presence of scattering between the local Mott liquid and the local non-Fermi liquid states.

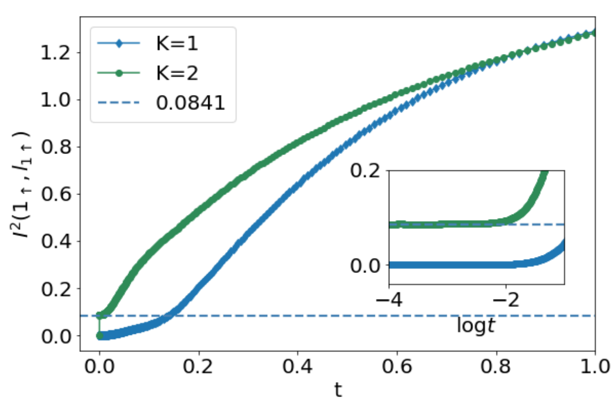

FIG. 16. Variation of the mutual information $MI(1_{\sigma}, l_{1\sigma})$ between two nearest neighbor sites against t. The error-bar for the two channel case is $\sigma_2 \approx 0.005$.

Apart from these, we have also computed an intra-channel tripartite information $I^3(1_{\uparrow}, l_{1\uparrow}, l_{1\downarrow})$ of the two-channel ground state (blue curve in Fig. 17) - it shows that there is a discontinuity in the tripartite information at $t = 0^{+}$, and at low hopping strength the tripartite information is independent of t with a value 0.084. This non-zero value of the tripartite information is consistent with the presence of a non-Fermi liquid effective Hamiltonian having more than just two-particle interactions within it. We have also studied inter-channel mutual information $I^2(1_{\uparrow}, 2_{\uparrow})$ for $K = 2$ (red curve in fig. 17). It reveals the correlation and quantum entanglement between these two channels, and demonstrates the all-to-all nature of the local Mott liquid.

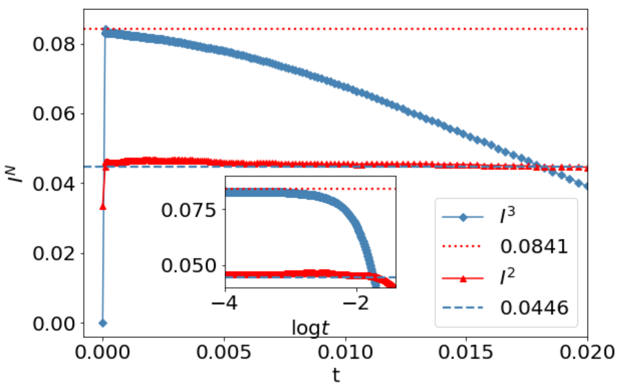

FIG. 17. Red: Mutual information $I^2(1_\uparrow, 2_\uparrow)$ against t. Blue: Tripartite information $I^3(1_\uparrow, l_{1\uparrow}, l_{1\downarrow})$ against t. The error-bar (σ) for the I^3 and I^2 near the low hopping strength are 0.002 and 0.003 respectively.

3. *Bures distance and the orthogonality catastrophe*

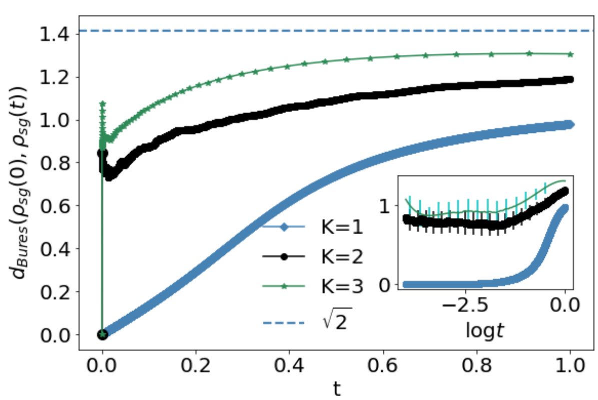

FIG. 18. Variation of Bures distance between the reduced density matrices of the star graph ground states at $t = 0$ and $t \neq 0$, against t. The error-bars (σ) for $K = 2$ and $K = 3$ are 0.14 and 0.08 respectively, and near $t \approx 1$ the σ are 0.04 and 0.07 respectively.

In addition to these entanglement measures, we have also calculated the Bures distance between the states at $t = 0$ and $t > 0$. The Bures distance [101–106] between two density matrices ρ_1, ρ_2 is defined as

$$d_{Bures}(\rho_1, \rho_2) = \sqrt{2}\left[1 - \mathrm{Tr}\left\{\left(\rho_1^{1/2}\rho_2\rho_1^{1/2}\right)^{1/2}\right\}\right] , \quad (58)$$

and is a measure of the distance, in the Hilbert space, between the states forming the density matrices. One can see from the above definition that the maximum and minimum possible distances are $\sqrt{2}$ and 0 respectively.

We get the ground state $|\psi(t)\rangle$ of the problem by solving the Hamiltonian in Eq. (40). This ground state $|\psi(t)\rangle(t)$ and the associated density matrix $\rho(t) = |\psi(t)\rangle\langle\psi(t)|$ are functions of the hopping strength t. We are interested in the reduced density matrix $\rho_{sg}(t)$ of only the sites that form the star graph (impurity site and the zeroth sites of the conduction channels), so we trace out all the nearest neighbor sites from the full density matrix:, $\rho_{sg}(t) = \mathrm{Tr}_{n-n}(\rho(t))$. The Bures distance $d_{Bures}(\rho_{sg}(0), \rho_{sg}(t))$ is then calculated between the reduced density matrices at $t = 0$ and $t > 0$, for $K = 1$, $K = 2$ and $K = 3$.

We have shown the variation of the Bures distance as a function of the hopping strength t in Fig. 18. Although the Bures distance is 0 (by definition) at $t = 0$ for all K, a difference arises as t is made slightly non-zero: there is a discontinuity in the Bures distance for the two and three channel models, while the single channel Bures distance is continuous. The smooth variation of the Bures distance in the single channel case shows the adiabatic continuity of the reduced star graph density matrix from the $t = 0$ case to $t \neq 0$ case. On the other hand, the abrupt jump in the Bures distance for higher-channel cases at $t = 0^+$ shows the breakdown of adiabatic continuity between the $t = 0$ and $t = 0^+$ Hamiltonians and signals an *orthogonality catastrophe* between these two ground states. The discontinuity increases as K is increased, indicating that taking more channels will lead to the maximum Bures distance of $d_{Bures} = \sqrt{2}$ and hence an exact orthogonality.

VI. DUALITIES OF THE MCK MODEL

We start from a strong coupling ($J \to \infty$) spin-S impurity MCK Hamiltonian in the over-screened regime ($K > 2S$),

$$H(J) = \sum_{k,\sigma,l} \epsilon_{k,l}\hat{n}_{k\sigma,l} + J\vec{S_d}\cdot\vec{S} \ . \quad (59)$$

Here, $\vec{S}$ is the total spin $\sum_l \sum_{kk'\alpha\beta} \vec{\sigma}_{\alpha\beta} c^\dagger_{k\alpha,l} c_{k'\beta,l}$ of all the zero modes. At strong coupling, the ground states of the star graph eq. 8 act as a good starting point for a perturbative expansion. As argued previously, there are $K - 2S_d + 1$ ground states, labeled by the K values of the total spin angular momentum $J^z = S^z_d + S^z = -\frac{K}{2} + S_d, -\frac{K}{2} + S_d + 1, \ldots, \frac{K}{2} - S_d$. Since a general spin-$s$ object is simply a $2s+1$ level system, the $K-$fold degenerate ground state manifold can be used to define a new impurity spin $\mathbb{S}_d$ of multiplicity $2\mathbb{S}_d + 1 = K - 2S_d + 1$ which implies that we need $\mathbb{S}_d = \frac{K}{2} - S_d$. That is, the spin-$S_d$ impurity has a dual described by a spin-$(K - 2S_d + 1)$ impurity. The states of this new spin are defined by

$$\hat{\mathbb{S}_d^z} \left| S^z \right\rangle = S^z \left| S^z \right\rangle ,$$
$$\hat{\mathbb{S}_d^{\pm}} \left| S^z \right\rangle = \sqrt{\mathbb{S}_d \left(\mathbb{S}_d + 1\right) - S^z \left(S^z \pm 1\right)} \left| S^z \pm 1 \right\rangle \ . \quad (60)$$

While the ground state subspace gives rise to the new central spin object, the excited states of the star graph can be used to define bosonic operators that mediate interactions between the central spin and the next-nearest neighbour lattice sites [85]. In terms of the zero-bandwidth spectrum, the bosonic operators represent scattering between the ground state subspace and the excited subspaces. Through a Schrieffer-Wolff transformation in the small coupling $\frac{t^2}{J}$, one can then remove this interaction and generate an exchange-coupling between the new impurity $\vec{\mathbb{S}}_d$ and the new zero modes formed out of the remaining sites in the lattice [85] (by remaining, we mean those real space sites that have not been consumed into forming the new spin). The new Hamiltonian, characterized by the small super-exchange coupling $\mathbb{J}$ of the general form $\gamma t^2/J$, has the form

$$H'(\mathbb{J}) = \sum_{k,\sigma,l} \epsilon_{k,l} \hat{n}_{k\sigma,l} + \mathbb{J} \vec{\mathbb{S}_d} \cdot \vec{\mathbb{S}} \ . \quad (61)$$

$\vec{\mathbb{S}}$ is the local bath spin formed by the new zero modes. This Hamiltonian is very similar to the one in eq. 59, and that is the essence of the strong-weak duality: One can go from the over-screened strong coupling spin-S MCK model to another over-screened weak coupling spin-$(K - 2S + 1)$ MCK model. For the case of $K = 4S$, we have $\mathbb{S}_d = S_d$, and both S_d and $\mathbb{S}_d$ describe the same spin objects (at least formally). The two models are then said to be self-dual. For example, for the case of spin-half MCK model, two-channel model is self-dual.

One important consequence of the duality relationship between the two over-screened models is that the RG equations are also dual; while the strong coupling model has an irrelevant coupling $\mathcal{J}$ that flows down to the intermediate fixed point $\mathcal{J}^*$, the weak coupling model has a relevant coupling $\mathbb{J}$ that flows up to the same fixed point $\mathbb{J}^* = \mathcal{J}^*$. From the RG equation for the general spin-S MCK model, we know that $\mathbb{J}^* = \frac{2}{K\rho'}$, where ρ' is the DOS for the bath of the weak coupling Hamiltonian. This constrains the form of the scaling factor γ:

$$\mathbb{J}^* = \frac{\gamma 4t^2}{\mathcal{J}^*} = \frac{2}{K\rho'} \implies \gamma = \frac{1}{4t^2}{\mathcal{J}^*}^2 = \frac{1}{K^2 t^2 \rho\rho'} \ . \quad (62)$$

There exists another set of dual points in the MCK model. This was hinted at when we looked at the degree of compassion in eq. 12. Since Γ depends only on the magnitude of δ, both $\pm\delta$ will give the same degree of compensation, same ground state energy and same ground state degeneracy $\left(g_K^{S_d} = |\delta| + 1\right)$. The definition of δ gives the duality transformation as $K \to 2S_d, S_d \to \frac{K}{2}$. That is, we transform from a $K-$channel MCK model with spin-S_d impurity, to a $2S_d$-channel MCK with a spin-$\frac{K}{2}$ impurity. The exactly-screened model $K = 2S_d$ maps on to itself and is therefore self-dual under this transformation.

For $K \neq 2S_d$, we transform an over-screened model into an under-screened model and vice versa. This duality relationship allows us to infer the RG scaling behaviour of one of the models if we know that of the other. If we know that for a certain pair of values K and S_d, the $K-$channel MCK model with spin-S_d impurity has an intermediate fixed point, we can immediately conclude that the $2S_d$-channel spin-$\frac{K}{2}$ model has a strong coupling fixed point.

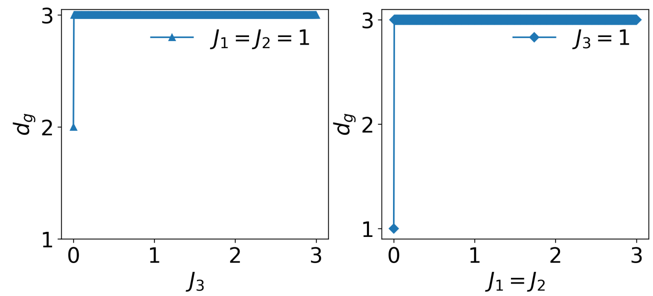

FIG. 19. *Left:* Variation of the ground state degeneracy against the J_3 keeping $J_1 = J_2 = 1$ fixed. *Right:* Variation of ground state degeneracy against $J_1 = J_2$ keeping J_3 fixed. Both plots show the robustness of the ground state degeneracy against channel anisotropy.

VII. QUANTUM PHASE TRANSITION IN THE MCK MODEL UNDER CHANNEL ANISOTROPY

For a channel-anisotropic MCK model with K Kondo couplings $\{\mathcal{J}_i\}$ for each of the K conduction channels, the zero bandwidth model is

$$H_K(\vec{\mathcal{J}}) \ = \ \sum_{i=1}^{K} \mathcal{J}_i \vec{S}_d.\vec{S}_i \ . \quad (63)$$

For the special case $\mathcal{J}_i = \mathcal{J}, \forall i$ we get the usual isotropic star graph model. For the case of spin-1/2 impurity, we find that the Hamiltonian with any value of $\mathcal{J}_i > 0$ has K fold ground state degeneracy. This shows that the ground state degeneracy of the star graph model is extremely robust against the channel anisotropy; the ground state degeneracy does not change until at least one $\mathcal{J}_i$ vanishes.

We have demonstrated this numerically for a three channel anisotropic star graph model. In Fig. 19(a), we show that if two couplings are kept fixed to be equal ($\mathcal{J}_1 = \mathcal{J}_2 = 1$) and the third coupling $\mathcal{J}_3$ is tuned from some finite value to zero, the degeneracy does not change from 3 to 2 until $\mathcal{J}_3$ becomes zero. At that point, the model becomes a two channel Kondo problem. We also show in Fig. 19(b) that we keep the first coupling $\mathcal{J}_3$ fixed to 1 and vary the common coupling $\mathcal{J}_1 = \mathcal{J}_2$ from non-zero to zero, this is equivalent to keeping $\mathcal{J}_1 = \mathcal{J}_2 = 1$ fixed and taking $\mathcal{J}_1$ to infinity from finite. In this case we find when the coupling $\mathcal{J}_1 = \lambda_2 = 0$ the degeneracy becomes one showing the effective single channel nature.

The above demonstration makes it clear that the ground state degeneracy can change only when at least one of the Kondo couplings vanish. This can be realised under RG flow if one considers the anisotropic MCK model.

$$H = \sum_{k,\alpha,l} \epsilon_{k,l} \hat{n}_{k\alpha,l} + \sum_{\substack{kk',\\ \alpha,\beta,l}} \mathcal{J}_l \vec{S}_d \cdot \frac{1}{2} \vec{\sigma}_{\alpha\beta} c^\dagger_{k\alpha,l} c_{k'\beta,l} \ . \quad (64)$$

We consider the specific case where $K-1$ channels have the same coupling $\mathcal{J}_1 = \mathcal{J}_2 = ... = \mathcal{J}_{K-1} = \mathcal{J}_+$ and the remaining channel has a different coupling $\mathcal{J}_K = \mathcal{J}_-$. The RG equations for such a model are

$$\frac{\Delta \mathcal{J}_\pm}{|\Delta D|} = -\frac{\mathcal{J}_\pm^2 \rho}{\mathcal{D}_\pm} + \frac{\rho^2 \mathcal{J}_\pm}{2} \left[\frac{(K-1)\mathcal{J}_+^2}{\mathcal{D}_+} + \frac{\mathcal{J}_-^2}{\mathcal{D}_-} \right] \ , \quad (65)$$

where $\mathcal{D}_\pm = \omega - \frac{D}{2} - \frac{\mathcal{J}_\pm}{4}$ are the denominators of the URG equations. Setting $\mathcal{J}_+ = \mathcal{J}_-$ leads to the critical fixed point at $\mathcal{J}_+^* = \mathcal{J}_-^* = \mathcal{J}_* = \frac{2}{K\rho}$. We now perturb around this fixed point by defining new variables $j_\pm = \mathcal{J}_\pm - \mathcal{J}_*$. We also assume that the bandwidth is large enough so that $\mathcal{D}_\pm \simeq \omega - \frac{D}{2} - \frac{\mathcal{J}_*}{4} = -|\mathcal{D}_*|$. Performing a linear stability analysis about $j_\pm = 0$ then reveals the following two possibilities:

(a) If $j_- < 0, j_+ > 0$, the deviation j_- is relevant and $\mathcal{J}_-$ flows to zero. The flow of j_+ are constrained such that the remaining couplings $\mathcal{J}_+$ flow to the stable intermediate fixed point of the $K-1$ channel MCK model: $J_{+,*} = \frac{2}{(K-1)\rho}$.

(b) If $j_- > 0, j_+ < 0$, the couplings $\mathcal{J}_+$ are irrelevant, and this leads to a single channel Kondo model described by the coupling $\mathcal{J}_-$ which flows to strong coupling.

These conclusions show that the K channel intermediate fixed point is unstable under channel anisotropy [14, 32, 37, 45]. If one of the couplings becomes smaller than the rest, then that coupling flows to zero while the other $K-1$ couplings flow to the $K-1$ channel fixed point. On the other hand, if $K-1$ couplings are smaller than a single coupling, then the smaller couplings vanish while the remaining coupling flows to strong-coupling.

VIII. CONCLUSIONS

In summary, we have explored the low-energy behaviour of the MCK models using the unitary renormalization group (URG) method and obtained a better understanding of the role of ground state degeneracy and quantum-mechanical frustration in shaping the non-Fermi liquid physics and criticality. Using the unitary renormalization group technique, we have obtained the zero-temperature phase diagram of the MCK problem and an effective Hamiltonian with a simple zero bandwidth limit - the star graph, and it determines the ground state energy, wavefunction and degeneracy of the MCK models. This star graph is found to explain much of the physics of over-screening and criticality, including the singularities in the susceptibility and magnetisation, as well as a reduction in the degree to which the impurity spin is compensated. The overarching message there was that the ground state degeneracy of the star graph (which is unity for single-channel and greater for the over-screened models) was the key ingredient in leading to the qualitative and quantitative differences from the single-channel model The presence of ground state degeneracy also allows the construction of non-local twist operators and fractional excitations in the ground state manifold. Integrating out the quantum fluctuations of the impurity leads to an all-to-all effective Hamiltonian for the local bath spins, and the Hamiltonian is found to contain inter-channel quantum scattering in terms of electron-hole pairs, thereby creating a local Mott-liquid phase at the origin of the lattice.

The low energy effective Hamiltonian (LEH) for the excitations is then obtain by considering fluctuations of the conduction bath on top of the ground state. The LEH for the 2-channel Kondo confirms absence of any Fermi liquid phase due to an exact cancellation across the ground state manifold, and the presence of inter-channel off-diagonal non-Fermi liquid terms. Our analysis reinforces the idea that the ground state degeneracy is crucial to the non-Fermi liquid physics and to the presence of such off-diagonal terms in the LEH. The existence of a marginal Fermi liquid within the effective Hamiltonian clearly displays the orthogonality catastrophe in the form of singularities that are absent at exact screening. Studies of various thermodynamic properties (presented in the Supplementary Material [73]) from this 2-channel Kondo LEH like specific heat and susceptibility show logarithmic dependence at low temperature, in agreement with the literature [8, 30–35, 42–46].

The non-diagonal nature of the LEH is further investigated through the several measures of entanglement. The entanglement entropy, calculated from the minimum J^z states, between the impurity and the outer spins, as well as between an outer spin and the rest saturate to $\ln 2$ in the large channel limit saturate. The opposite behaviour happens in the maximum J^z state, where the entanglement entropy decreases with the increase of channel number. The large values of inter-channel mutual information indicate high inter-channel correlation in the MCK ground state. The power-law dependence of the multi-partite information among the outer spins of the star graph model is similar to the power-law behavior of the all-to-all local Mott-liquid ground state. The presence of a discontinuity in the non-Fermi liquid ground state multi-channel entanglement as compared to the smooth behaviour in the single-channel counterpart again points to the orthogonality catastrophe in the low-energy phase of the multi-channel models. Higher discontinuity for a higher number of channels was observed in the Bures distance study. The URG study of the channel anisotropic MCK shows the critical and unstable nature of the isotropic fixed point; under any anisotropic perturbations, the RG flows go towards either the single-channel model or the symmetric MCK with one less channel coupled to the impurity. This is complemented by the study of the star graph ground state degeneracy which shows that the degeneracy changes only if one or more couplings vanishes. When combined, we can conclude that in the presence of channel anisotropy, the degeneracy of the MCK ground state does not change until the RG reaches the stable fixed point.

This method serves as a template for the study of other quantum impurity systems. We have already seen that the degeneracy of the star graph is robust under anisotropy; one can perform similar studies in the presence of a superconducting gap that cuts off the ground state manifold from the excitations, hence providing the degeneracy a topological protection. The duality transformations then allow us to view the topologically protected ground state as a larger quantum spin which is essentially isolated. This holds immense potential for applications in quantum information and quantum computation. More fine-tuned behaviour can be obtained by studying the MCK model with an easy-axis anisotropy term $\left(J^i\right)^2$ along one of the axes (i). Such a term would, if it is able to survive the RG flows towards low energy, lift the degeneracy of the ground state and make it possible to achieve perfect screening even with $K > 2S_d$. One can also study the multi-channel lattice models [107, 108] to better understand the role played by singlet frustration and ground state degeneracy in the competition between the local moment versus the heavy fermion sea.

ACKNOWLEDGMENTS

SP and Anirban Mukherjee thanks the CSIR, Govt. of India and IISER Kolkata for funding through a research fellowship. Abhirup Mukherjee thanks IISER Kolkata for funding through a research fellowship. S. Lal thanks the SERB, Govt. of India for funding through MATRICS grant MTR/2021/000141 and Core Research Grant CRG/2021/000852.

[1] A. C. Hewson, The Kondo Problem to Heavy Fermions (Cambridge University Press, 1993).
[2] P. W. Anderson and G. Yuval, Physical Review Letters **23**, 89 (1969).
[3] P. W. Anderson, G. Yuval, and D. Hamann, Physical Review B **1**, 4464 (1970).
[4] P. W. Anderson, Journal of Physics C: Solid State Physics **3**, 2436 (1970).
[5] K. G. Wilson, Rev. Mod. Phys. **47**, 773 (1975).
[6] N. Andrei, K. Furuya, and J. H. Lowenstein, Rev. Mod. Phys. **55**, 331 (1983).
[7] A. M. Tsvelick and P. B. Wiegmann, Adv. in Phys. **32**, 453 (1983).
[8] I. Affleck and A. W. Ludwig, Physical Review B **48**, 7297 (1993).
[9] I. Affleck, Acta Phys.Polon.B **26** (1995).
[10] P. Nozieres, Journal of Low Temperature Physics **17**, 31 (1974).
[11] A. C. Hewson, Advances in Physics **43** (1994).
[12] J. Kondo, Progress of Theoretical Physics **32**, 37 (1964), https://academic.oup.com/ptp/article-pdf/32/1/37/5193092/32-1-37.pdf.
[13] Y. hui Zhang, S. Kahle, T. Herden, C. Stroh, M. Mayor, U. Schlickum, M. Ternes, P. Wahl, and K. Kern, Nature Communications **4** (2013), 10.1038/ncomms3110.
[14] Nozières, Ph. and Blandin, A., J. Phys. France **41**, 193 (1980).
[15] I. Affleck and A. W. W. Ludwig, Phys. Rev. Lett. **68**, 1046 (1992).
[16] I. Affleck, A. W. W. Ludwig, and B. A. Jones, Phys. Rev. B **52**, 9528 (1995).
[17] A. Georges and Y. Meir, Phys. Rev. Lett. **82**, 3508 (1999).
[18] G. Zaránd, C.-H. Chung, P. Simon, and M. Vojta, Phys. Rev. Lett. **97**, 166802 (2006).
[19] A. K. Mitchell, D. E. Logan, and H. R. Krishnamurthy, Phys. Rev. B **84**, 035119 (2011).
[20] A. K. Mitchell, E. Sela, and D. E. Logan, Phys. Rev. Lett. **108**, 086405 (2012).
[21] E. J. König, P. Coleman, and Y. Komijani, Phys. Rev. B **104**, 115103 (2021).
[22] P. Coleman, Phys. Rev. B **35**, 5072 (1987).
[23] A. J. Millis and P. A. Lee, Phys. Rev. B **35**, 3394 (1987).
[24] A. Auerbach and K. Levin, Phys. Rev. Lett. **57**, 877 (1986).
[25] T. M. Rice and K. Ueda, Phys. Rev. B **34**, 6420 (1986).
[26] G. R. Stewart, Rev. Mod. Phys. **56**, 755 (1984).
[27] M. Granath and H. Johannesson, Phys. Rev. B **57**, 987 (1998).
[28] A. Zawadowski, Phys. Rev. Lett. **45**, 211 (1980).
[29] D. L. Cox and A. Zawadowski, Advances in Physics **47**, 599 (1998), https://doi.org/10.1080/000187398243500.
[30] I. Affleck and A. W. Ludwig, Nuclear Physics B **360**, 641 (1991).
[31] A. W. W. Ludwig and I. Affleck, Phys. Rev. Lett. **67**, 3160 (1991).
[32] I. Affleck, A. W. W. Ludwig, H.-B. Pang, and D. L. Cox, Phys. Rev. B **45**, 7918 (1992).
[33] O. Parcollet and A. Georges, Phys. Rev. Lett. **79**, 4665 (1997).
[34] I. Affleck, Journal of the Physical Society of Japan **74**, 59 (2005), https://doi.org/10.1143/JPSJ.74.59.
[35] V. J. Emery and S. Kivelson, Phys. Rev. B **46**, 10812 (1992).
[36] D. G. Clarke, T. Giamarchi, and B. I. Shraiman, Phys. Rev. B **48**, 7070 (1993).

[37] G. Zaránd and J. von Delft, Phys. Rev. B **61**, 6918 (2000).
[38] J. von Delft, G. Zaránd, and M. Fabrizio, Phys. Rev. Lett. **81**, 196 (1998).
[39] A. J. Schofield, Phys. Rev. B **55**, 5627 (1997).
[40] R. Bulla, T. A. Costi, and T. Pruschke, Rev. Mod. Phys. **80**, 395 (2008).
[41] H. B. Pang and D. L. Cox, Phys. Rev. B **44**, 9454 (1991).
[42] N. Andrei and C. Destri, Phys. Rev. Lett. **52**, 364 (1984).
[43] A. M. Tsvelick and P. B. Wiegmann, Zeitschrift für Physik B Condensed Matter **54**, 201 (1984).
[44] A. M. Tsvelick, Journal of Physics C: Solid State Physics **18**, 159 (1985).
[45] N. Andrei and A. Jerez, Phys. Rev. Lett. **74**, 4507 (1995).
[46] G. Zaránd, T. Costi, A. Jerez, and N. Andrei, Phys. Rev. B **65**, 134416 (2002).
[47] A. M. Sengupta and A. Georges, Phys. Rev. B **49**, 10020 (1994).
[48] M. Fabrizio, A. O. Gogolin, and P. Nozières, Phys. Rev. Lett. **74**, 4503 (1995).
[49] P. Coleman, L. B. Ioffe, and A. M. Tsvelik, Phys. Rev. B **52**, 6611 (1995).
[50] M. Fabrizio, A. O. Gogolin, and P. Nozières, Phys. Rev. B **51**, 16088 (1995).
[51] A. V. Rozhkov, International Journal of Modern Physics B **12**, 3457 (1998), https://doi.org/10.1142/S0217979298002805.
[52] R. Zheng, R.-Q. He, and Z.-Y. Lu, Phys. Rev. B **103**, 045111 (2021).
[53] K. Vladár and A. Zawadowski, Phys. Rev. B **28**, 1564 (1983).
[54] T. Cichorek, A. Sanchez, P. Gegenwart, F. Weickert, A. Wojakowski, Z. Henkie, G. Auffermann, S. Paschen, R. Kniep, and F. Steglich, Phys. Rev. Lett. **94**, 236603 (2005).
[55] D. C. Ralph and R. A. Buhrman, Phys. Rev. Lett. **69**, 2118 (1992).
[56] D. C. Ralph, A. W. W. Ludwig, J. von Delft, and R. A. Buhrman, Phys. Rev. Lett. **72**, 1064 (1994).
[57] Z. Iftikhar, S. Jezouin, A. Anthore, U. Gennser, F. D. Parmentier, A. Cavanna, and F. Pierre, Nature **526**, 233 (2015).
[58] L. J. Zhu, S. H. Nie, P. Xiong, P. Schlottmann, and J. H. Zhao, Nature Communications **7**, 10817 (2016).
[59] R. M. Potok, I. G. Rau, H. Shtrikman, Y. Oreg, and D. Goldhaber-Gordon, Nature **446**, 167 (2007).
[60] A. J. Keller, L. Peeters, C. P. Moca, I. Weymann, D. Mahalu, V. Umansky, G. Zaránd, and D. Goldhaber-Gordon, Nature **526**, 237 (2015).
[61] V. Emery and S. Kivelson, Nature **374**, 434 (1995).
[62] H. T. Mebrahtu, I. V. Borzenets, H. Zheng, Y. V. Bomze, A. I. Smirnov, S. Florens, H. U. Baranger, and G. Finkelstein, Nature Physics **9**, 732 (2013).
[63] B. Alkurtass, A. Bayat, I. Affleck, S. Bose, H. Johannesson, P. Sodano, E. S. Sørensen, and K. Le Hur, Phys. Rev. B **93**, 081106 (2016).
[64] D. Kim, J. Shim, and H.-S. Sim, Phys. Rev. Lett. **127**, 226801 (2021).
[65] A. Mukherjee and S. Lal, Nuclear Physics B **960**, 115170 (2020).
[66] A. Mukherjee and S. Lal, Nuclear Physics B **960**, 115163 (2020).
[67] A. Mukherjee, A. Mukherjee, N. S. Vidhyadhiraja, A. Taraphder, and S. Lal, Phys. Rev. B **105**, 085119 (2022).
[68] S. Pal, A. Mukherjee, and S. Lal, **21**, 023019 (2019).
[69] S. P. Anirban Mukherjee and S. Lal, Journal of High Energy Physics **2021** (2021), 10.1007/JHEP04(2021)148.
[70] A. Mukherjee and S. Lal, New Journal of Physics **22**, 063007 (2020).
[71] A. Mukherjee and S. Lal, New Journal of Physics **22**, 063008 (2020).
[72] S. Patra and S. Lal, Phys. Rev. B **104**, 144514 (2021).
[73] See the Supplementary Materials available online for this work.
[74] J. Gan, **6**, 4547 (1994).
[75] E. Kogan, Journal of Physics Communications **2**, 085001 (2018).
[76] Y. Kuramoto, The European Physical Journal B - Condensed Matter and Complex Systems **5**, 457 (1998).
[77] A. M. Tsvelick and P. B. Wiegmann, Zeitschrift für Physik B Condensed Matter **54**, 201 (1984).
[78] A. K. Mitchell, M. R. Galpin, S. Wilson-Fletcher, D. E. Logan, and R. Bulla, Phys. Rev. B **89**, 121105 (2014).
[79] V. Tripathi, Landau Fermi Liquids and Beyond (CRC Press, 2018).
[80] E. Fradkin, Field theories of condensed matter physics (Cambridge University Press, 2013).
[81] C. M. Varma and Y. Yafet, Phys. Rev. B **13**, 2950 (1976).
[82] K. Yosida, Phys. Rev. **147**, 223 (1966).
[83] K. G. Wilson, Reviews of Modern Physics **47**, 773 (1975).
[84] C. P. Moca, I. Weymann, M. A. Werner, and G. Zaránd, Phys. Rev. Lett. **127**, 186804 (2021).
[85] C. Kolf and J. Kroha, Phys. Rev. B **75**, 045129 (2007).
[86] R. Žitko and M. Fabrizio, Phys. Rev. B **95**, 085121 (2017).
[87] J. Gan, N. Andrei, and P. Coleman, Phys. Rev. Lett. **70**, 686 (1993).
[88] A. M. Tsvelick and P. B. Wiegmann, Journal of Statistical Physics **38**, 125 (1985).
[89] T. Kimura and S. Ozaki, Journal of the Physical Society of Japan **86**, 084703 (2017), https://doi.org/10.7566/JPSJ.86.084703.
[90] D. Bensimon, A. Jerez, and M. Lavagna, Phys. Rev. B **73**, 224445 (2006).
[91] D. L. Cox and M. Jarrell, **8**, 9825 (1996).
[92] P. Coleman and C. Pépin, Phys. Rev. B **68**, 220405 (2003).
[93] N. Roch, S. Florens, T. A. Costi, W. Wernsdorfer, and F. Balestro, Phys. Rev. Lett. **103**, 197202 (2009).
[94] A. Schiller and L. De Leo, Phys. Rev. B **77**, 075114 (2008).
[95] P. Durganandini, EPL (Europhysics Letters) **95**, 47003 (2011).
[96] K. Tandon, S. Lal, S. K. Pati, S. Ramasesha, and D. Sen, Phys. Rev. B **59**, 396 (1999).
[97] C. Varma, Z. Nussinov, and W. Van Saarloos, Physics Reports **361**, 267 (2002).
[98] P. W. Anderson, Phys. Rev. Lett. **18**, 1049 (1967).
[99] K. Yamada and K. Yosida, Progress of Theoretical Physics **59**, 1061 (1978), https://academic.oup.com/ptp/article-pdf/59/4/1061/5315849/59-4-1061.pdf.

[100] K. Yamada and K. Yosida, Progress of Theoretical Physics **62**, 363 (1979).

[101] A. Uhlmann, Reports on Mathematical Physics **9**, 273 (1976).

[102] D. Bures, Transactions of the American Mathematical Society **135**, 199 (1969).

[103] M. Hübner, Physics Letters A **163**, 239 (1992).

[104] M. Hübner, Physics Letters A **179**, 226 (1993).

[105] J. Dittmann, Journal of Geometry and Physics **13**, 203 (1994).

[106] P. Marian, T. A. Marian, and H. Scutaru, Physical Review A **68**, 062309 (2003).

[107] C. A. Piguet, D. F. Wang, and C. Gruber, Journal of Low Temperature Physics **106**, 3 (1997).

[108] M. Shaw, X.-w. Zhang, and D. Jin, Phys. Rev. B **57**, 8381 (1998).